Canadian Mineralogist
Vol. 26, pp. 765-786 (1988)

GEYSER-TYPE DISCHARGE IN ATLANTIS II DEEP, RED SEA: EVIDENCE OF BOILING FROM FLUID INCLUSIONS IN EPIGENETIC ANHYDRITE*

CLAIRE RAMBOZ
Centre de Recherches Pétrographiques et Géochimiques, B.P. 20, 54501-Vandoeuvre-lès-Nancy, France

ELISABETH OUDIN AND YVES THISSE**
B.R.G.M., avenue de Concyr, BP 6009, 45060-Orléans Cedex, France

ABSTRACT

Anhydrite crystals in veins at the base of a drill core from SW Basin sediment, Atlantis II Deep, Red Sea, contain in their core tubular primary two-phase aqueous inclusions which are either liquid- or vapor-dominant (type *L* and *V*, respectively). Type-*L* inclusions yield melting points of ice (T_{ml}) of between -20.4 and -4.4°C, and homogenization temperatures to liquid [T_h *L*–*V*(*L*)] in the range 55 to 420°C. Type-*V* inclusions show T_{ml} values between -12 and -5°C, and T_h *LV*(*V*) values between 324 and 430°C. Some crystal overgrowths contain more isometric NaCl-saturated primary inclusions. These are characterized by melting points of halite and T_h *LV*(*L*) values ranging from 50 to 283°C and 185 to 405°C, respectively; some supersaturated inclusions are characterized by T_h *LV*(*L*) values between 84 and 404°C. Type-*L* inclusions from crystal cores, with salinities <19 wt.% equiv. NaCl, show a decreasing salt content with increasing molar volume. Such $\overline{V}$–*X* properties are characteristic of inclusions containing heterogeneous mixtures of liquids and vapors generated by boiling; these inclusions were slightly cooled before trapping. Type-*L* inclusions with salinities in the range 19–23 wt.% equiv. NaCl result from homogeneous trapping. They consist of four populations with lognormal distributions of the T_{ml} values, and define four vertical trends in a $\overline{V}$–*X* plot which are parallel to those defined by saturated and supersaturated inclusions. Two inclusions from these trends, with maximum T_h values of 388 and 403°C and salinities of 21.3 and 32.6 wt.% equiv. NaCl, respectively, yield an internal pressure at $T = T_h$ which is within 10 bars of the *in situ* hydrostatic pressure on the seafloor (*i.e.*, 223 ±2 bars); this indicates that boiling took place. The fluid-inclusion data are consistent with an initial brine of ≈19 wt.% equiv. NaCl, and with an enthalpy around 1950 J/g, which became enriched in salt to ≈33 wt.% equiv. NaCl through loss of vapor. Near-isothermal long-duration boiling of solutions implies a deep fluid reservoir with a limited volume, and heated by a magma. The salt-enriched liquids were injected intermittently on the seafloor, then cooled without mixing. These data and mineralogical observations suggest that epigenetic anhydrite is the product of interaction of the fluid and the hematitic sediment, *i.e.*, of redox reactions involving Fe^{2+}/Fe^{3+} and $\Sigma S^{2-}/\Sigma SO_4^{2-}$.

Keywords: fluid inclusions, epigenetic anhydrite, boiling, hydrothermal metamorphism, Atlantis II Deep, Red Sea.

SOMMAIRE

Les cristaux d'anhydrite provenant de veines sécantes dans une carotte de sédiment du bassin SW de la fosse d'Atlantis II (mer Rouge), contiennent en leur coeur des inclusions aqueuses tubulaires primaires, à remplissage de liquide ou de vapeur dominant (type *L* et *V*, respectivement). Les inclusions de type *L* ont des températures de fusion de la glace (T_{ml}) comprises entre –20.4 et –4.4°C, et s'homogénéisent en phase liquide entre 55 et 420°C (T_h *LV*(*L*)). Les inclusions de type *V* ont des valeurs de T_{ml} comprises entre –12 et –5°C et des T_h *LV*(*V*) entre 324 et 430°C. Certains cristaux présentent des surcroissances avec des inclusions primaires isodiamétriques saturées en NaCl. Elles fournissent des températures de fusion de la halite et des valeurs de T_h*LV*(*L*) respectivement comprises entre 50 à 283°C et entre 185 à 405°C; les inclusions sursaturées en NaCl ont fourni des valeurs de T_h *LV*(*L*) comprises entre 84 et 404°C. Les inclusions de type *L* au coeur des cristaux, dont la salinité est <19% pds eq. NaCl, ont un contenu en NaCl qui décroit alors que leur volume molaire croit. De telles propriétés caractérisent des inclusions ayant piégé des mélanges mécaniques de liquide et de vapeur lors d'un processus d'ébullition; ces mélanges étaient déjà refroidis lors du piégeage. Les inclusions de type *L*, dont la salinité est comprise entre 19 et 23% pds., ont piégé un fluide homogène. Elles regroupent 4 populations montrant une distribution lognormale des T_{ml}, et définissent dans le plan $\overline{V}$–*X* 4 dérives verticales qui sont parallèles à celles définies par les inclusions saturées et sursaturées en NaCl. Deux inclusions appartenant à ces dérives, avec des T_h maximales de 388 et 403°C et une salinité égale à 21.3 et 32.6% pds., ont une pression interne à $T = T_h$ qui est à 10 bars près la pression du piégeage au fond de la mer, soit 223 ±2 bars. Ces résultats démontrent que les fluides ont été piégés à l'ébullition. On peut en déduire que la saumure initiale avait une salinité de ≈19% pds., et une enthalpie de 1950 J/g. Ce liquide s'est enrichi en NaCl jusqu'à ≈33% pds. par perte de vapeur. Une ébullition prolongée quasi isotherme implique que le fluide en profondeur a un volume limité et est réchauffé par un magma. Les liquides de salinité croissante ont été injectés de façon intermittente, et se sont refroidis sans mélange. Les données sur les fluides et les minéraux suggèrent que l'anhydrite épigénétique s'est formée par réaction entre le fluide et le sédiment hématitique, impliquant les couples rédox Fe^{2+}/Fe^{3+} et $\Sigma S^{2-}/\Sigma SO_4^{2-}$.

Mots-clés: inclusions fluides, anhydrite épigénétique, ébullition, métamorphisme hydrothermal, fosse d'Atlantis II, mer Rouge.

* Contribution C.R.P.G. N°749.

** Present address: La Touche, Sambin, 41120-Les Montils, France

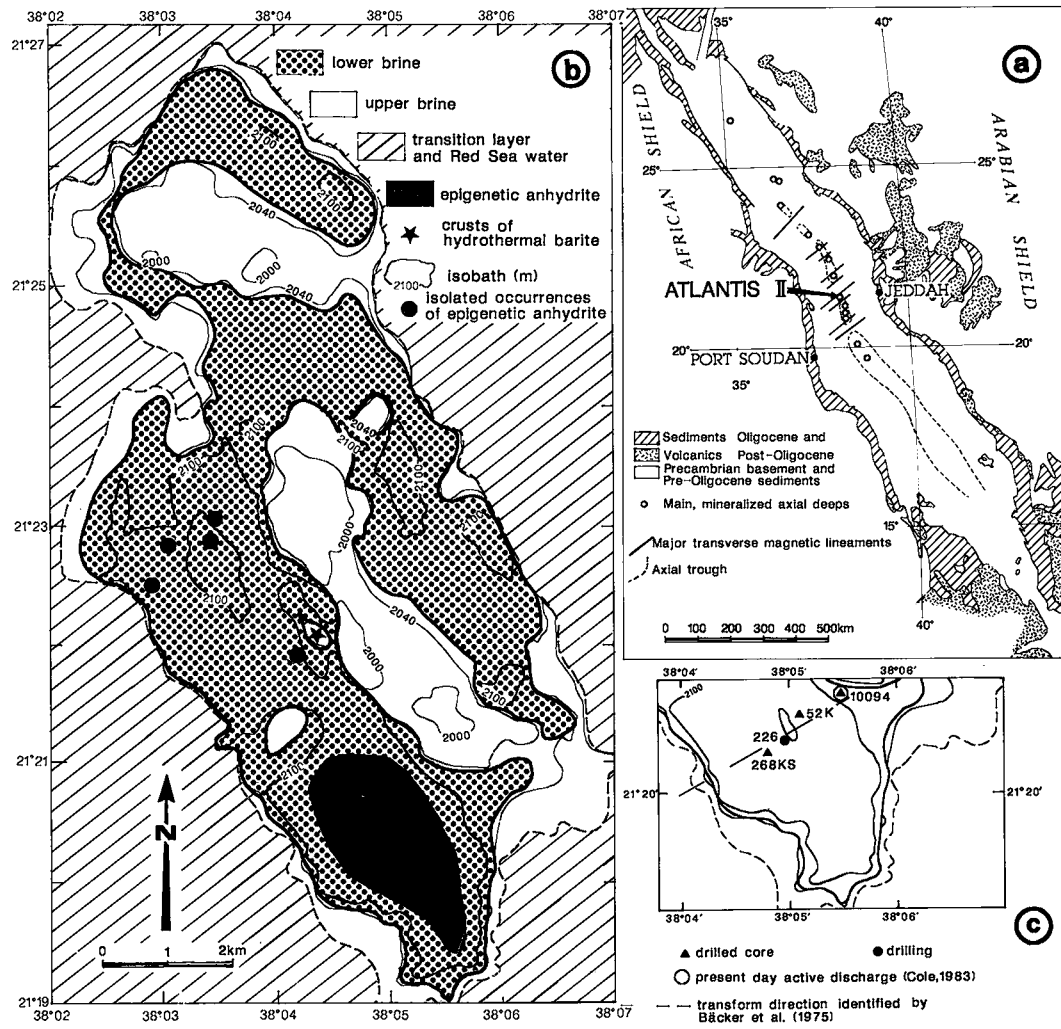

FIG. 1. (a) Schematic Red Sea map showing the mineralized Deeps close to transverse faults that crosscut the Axial Trough (after Bertin *et al.* 1979 and an unpublished compilation by Guennoc in Oudin *et al.* 1984). (b) Bathymetric map of Atlantis II Deep (depths are uncorrected for higher sound velocity in brines), showing surface areas covered by the lower and upper brines (situation in 1971; after Bäcker & Richter 1973). Sediments containing epigenetic anhydrite veins are after Zierenberg & Shanks (1983); hydrothermal barite crusts after Sval'nov *et al.* (1984). (c) Location of the studied 268 KS core, and other drill sites in SW Basin. 52K: core sample containing numerous epigenetic features (Zierenberg & Shanks 1983); 226: shallow basalt sequence (Ross *et al.* 1973); 10094: core showing evidence of present-day discharge (Cole 1983); 268 KS: core sampled at 21°20.45'N, 38°04.67'E (Thisse 1982, Oudin *et al.* 1984, this study).

INTRODUCTION

In the Atlantis II Deep, Red Sea (Fig. 1a), 10 to 30 m of metalliferous sediments have accumulated below anoxic stratified brines over the past 25,000 years. These form a potentially economic deposit of Zn, Ag, Au and Cd (Shanks 1983, Bäcker & Lange 1987). The brine pool in Atlantis II Deep is 14 km long, 5 km wide, and ~200 m thick (Fig. 1b). The pool consists of two convecting brine layers of nearly constant composition and temperature, separated by a 1-m-thick fluid interface, and overlain by a transition layer which, at the top, approaches the composition of deep Red Sea waters (Turner 1969, Hartmann 1980; Fig. 2). Experimental studies on double-diffusive layered brines show that such a

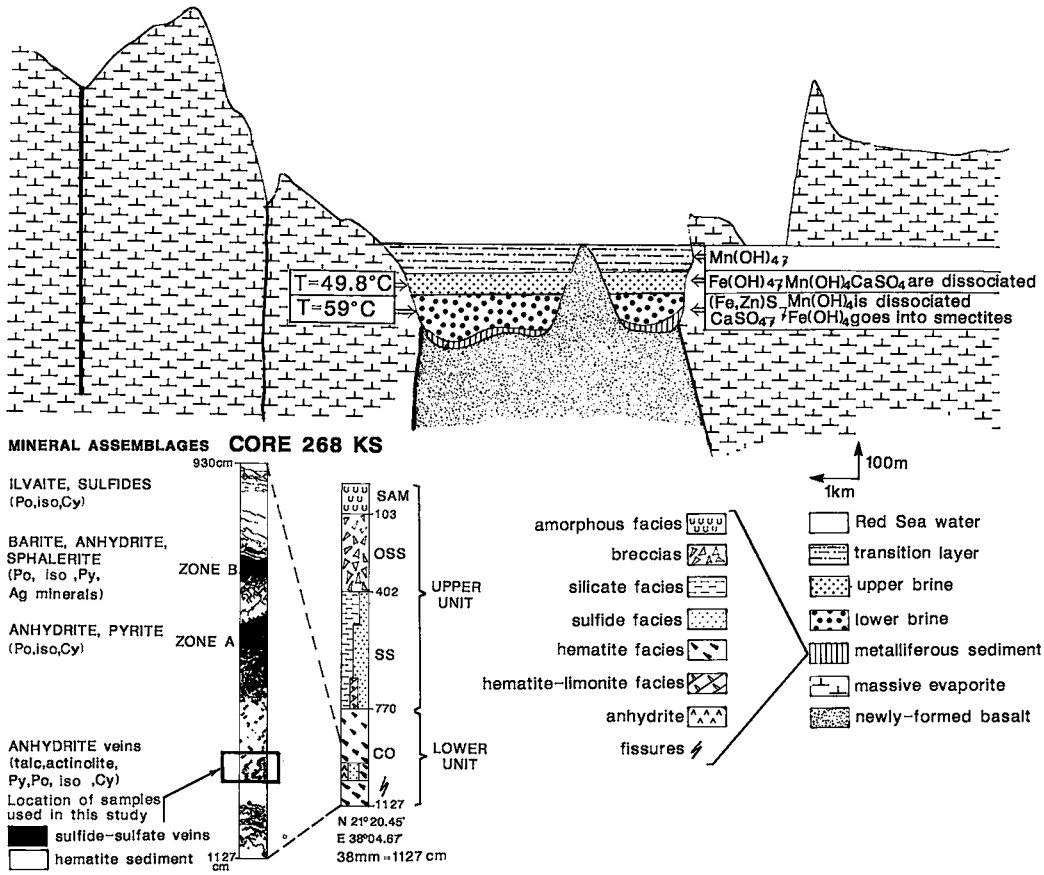

FIG. 2. Schematic cross-section of Atlantis II Deep (after Bäcker *et al.* 1975). The temperature of the stratified brines (situation in 1971) and the nature of the particulate matter they contain are schematic after Hartmann (1973, 1985), Cole (1983) and Zierenberg & Shanks (1986). The simplified stratigraphy of core 268 KS and an expanded section showing the location of the epigenetic anhydrite crystals examined in this study are at the bottom left (after Thisse 1982, Oudin *et al.* 1984). (Po pyrrhotite; Py pyrite; iso isocubanite; Cp chalcopyrite).

density-stratified structure is stable. Exchange through the lower interface is much more efficient for heat than for particulate matter (Turner 1969). Hydrological studies show that a vent source at the bottom of the SW Basin provides the whole Deep with hot brine, which homogenizes by convection (Schoell & Hartmann 1973; Fig. 1a). This accounts for the gradual increase in the temperature and volume of the lower brine observed for the past 15 years (Hartmann 1980). The lower brine is injected at the bottom of the Deep, with little or no mixing with seawater (Craig 1969, Turner 1969, Hartmann 1985). The upper brine, however, is a mixture of this lower brine with seawater (Craig 1969, Hartmann 1985).

Based on 300 cores collected in the Deep and its surroundings, the lithostratigraphy of the finely layered metalliferous sediments is, from bottom to top: detritic–oxidic pyritic zone (DOP), lower sulfidic zone (SU1), central oxidic zone (CO), upper sulfidic zone (SU2) and amorphous silicate zone (AM) (Bäcker & Richter 1973). All the units were deposited through rapid chemical sedimentation, with a small component of detrital material (Hackett & Bischoff 1973, Bäcker & Richter 1973, Shanks & Bischoff 1977). SW Basin core samples present a specific lithostratigraphy, due to intense brecciation, resedimentation and volcanic activity. These features are caused by the venting of hydrothermal sources in the SW Basin. This process started ≈11,000 years ago and still continues (Bäcker & Richter 1973). Numerous epigenetic veinlets or pseudoconformable beds indicate movement of hydrothermal solutions through the sediments (Bäcker & Richter 1973,

Zierenberg & Shanks 1983). These veins contain a complex assemblage of sulfides and anhydrite, similar to the high-temperature assemblages forming hydrothermal chimneys along the EPR (Oudin 1983, Oudin *et al.* 1984). The veins are associated with talc, ilvaite, actinolite, pyroxene and garnet, which are either primary (*i.e.*, directly precipitated from the fluid) or secondary (*i.e.*, resulting from metamorphism of the sediment) (Weiss *et al.* 1980, Pottorf & Barnes 1983, Oudin 1983, Zierenberg & Shanks 1983, Oudin *et al.* 1984). Figures 1 and 2 summarize bathymetric, hydrographic, and geological and geochemical conditions in the Atlantis II Deep.

The conditions of hydrothermal discharge in Atlantis II Deep are not understood fully because the hot discharging brine has never been directly sampled. That hydrothermal activity in Atlantis II Deep is intermittent is shown by annual changes in the temperature of the lower and upper brines (Schoell & Hartmann 1978, Hartmann 1980). Barite crusts on basalts from the flank of the Central Sill near the SW Basin (star in Fig. 1b), with rhythmic sulfur and oxygen isotopic compositions, also imply episodic venting at around 140–180°C in the Deep (Sval'nov *et al.* 1984). Hydrothermal discharge in Atlantis II Deep is turbulent (Schoell & Hartmann 1978, Voorhis & Dorson 1975) and is characterized by a high flow rate of about 278 kg s^{-1} (Hartmann 1980). Present hydrothermal activity in the Atlantis II Deep is therefore similar to that of surface geysers (Ross 1972, Schoell & Hartmann 1978). Subaerial geyser discharge is commonly accomplished by a vapor phase (White 1968). It has, however, not been demonstrated to date that the brines discharging in Atlantis II Deep were boiling.

The temperature of brine venting in the Atlantis II Deep is poorly constrained. A wide range of values has been obtained from mineral and isotopic geothermometers, and from heat- and mass-balance calculations (see reviews by Shanks & Bischoff 1977, Pottorf 1980). The former methods may lead to erroneous results if mineralogical and isotopic disequilibria prevailed. However, the changes in the temperature and volume of the lower brine over the past 15 years should provide accurate estimates of brine temperatures.

The distribution of dissolved sulfides and sulfates in the stratified brine pool is as yet not understood. The lower brine contains no detectable H_2S (Brewer & Spencer 1969) although the sulfide content of the sediment is greatest in brine-venting areas. Anhydrite is stable in the lower brine, as indicated by its presence as an authigenic mineral in the youngest sediments (Hartmann 1985). Detailed calculations using Pitzer's equations confirm that the lower brine is anhydrite-saturated (C. Monnin, pers. comm.). During the period of increasing hydrothermal activity, the sulfate content of the lower brine, which is controlled by the solubility product of anhydrite, decreased from 840 to 683 ppm (Hartmann 1985). It remains to be explained how the anoxic lower brine has a low H_2S content and is saturated with respect to anhydrite, whereas the upper brine, which contains $\approx$55% of a sulfate-bearing seawater component (Hartmann 1985, Zierenberg & Shanks 1986), is undersaturated.

Bäcker & Richter (1973) examined the distribution of anhydrite in Atlantis II Deep sediments in relation to the anomalous distribution of dissolved sulfates and sulfides in the stratified brine pool. Epigenetic anhydrite is abundant in the W and SW basins (Zierenberg & Shanks 1983, Fig. 1b) but is insignificant in sediments from the periphery of the lower brine pool, which are directly precipitated from the upper brine (Fig. 1b). As the lower brine is representative of the hydrothermal fluid discharging in the Deep, the spatial distribution of anhydrite over the Deep suggests that anhydrite precipitates directly from the Ca and sulfates in the hydrothermal fluid, and seawater is not a source of these elements. The increasing SO_4 content with depth of interstitial waters from one SW Basin core suggests a deep source of sulfates (Blanc 1987).

Fluid inclusions in seafloor hydrothermal deposits (*e.g.*, Le Bel & Oudin 1982, Kusakabe *et al.* 1982) can provide information on the temperature of formation and on the role of fluid mixing or unmixing during mineral precipitation. However, inclusions are rare in minerals from Atlantis II Deep sediments. Pottorf (1980) first reported several (liquid + vapor)-filled inclusions in anhydrite from the SW Basin. Most inclusions leaked during heating runs, but three, filled with a $\approx$25 wt.% equiv. NaCl-rich solution, homogenized into the liquid phase, implying a minimum temperature of formation of about 238°C at 200 bars. Zierenberg & Shanks (1983) noted the presence of NaCl-saturated (liquid + vapor)-filled inclusions in addition to two-phase inclusions in the epigenetic anhydrite.

This paper presents extensive data on fluid inclusions in epigenetic anhydrite from one core typical of SW Basin sediments. The present work is intended to further constrain the temperature of brine discharge in the Atlantis II Deep, and to explain the formation of epigenetic anhydrite in brine-venting areas.

Description of the Core

The anhydrite samples studied were selected from core 268 KS, collected in the center of the SW Basin (Figs. 1b,c) during the *Valdivia* cruise Va 29 in 1980. Since then, the core has been stored at 2°C. The core consists of 11 m of sediments, and did not intersect the basaltic basement. The sediments are enriched in hematite, and are intensely brecciated and cross-

cut by veins (Thisse 1982). The lithostratigraphy and mineralogy of the core are summarized in Figure 2. The upper part of the core is enriched in clays and Zn, Fe, Pb and Cu sulfides relative to the lower part, which is dominated by hematite (Oudin *et al.* 1984). The 3-m-thick Lower Unit (Fig. 2) is crosscut by numerous epigenetic veins and unconformable beds of well-crystallized sulfides and sulfates. Millimeter-long anhydrite and barite crystals, which are rich in fluid inclusions, are all located in the lower 2 m of the core. The sediment adjacent to the veins has been intensely thermally metamorphosed. Metamorphic minerals include ilvaite, hematite, actinolite and talc (Oudin *et al.* 1984; Fig. 2). The anhydrite samples studied are from veins that crosscut hematitic sediments at a depth of 1085 ±5 cm (Fig. 2). The crystals are associated with talc, actinolite, pyrite, pyrrhotite, isocubanite and chalcopyrite. Barite was not observed, and the surrounding sediment contains only ≈420 ppm Ba (Thisse 1982). The chemistry of the layer 1085 sediment is representative of the bulk of the Lower Unit: SiO_2, Cu, Zn, and Pb are depleted relative to the Upper Unit.

Analytical Procedure

About 100 platy anhydrite crystals were hand-picked from the core at 2°C, then kept at room temperature for up to 8 months. Reliable microthermometric data were obtained for 182 inclusions from 16 selected anhydrite crystals, using a Chaix-Meca heating–freezing stage (Poty *et al.* 1976). Inclusions without NaCl daughter crystals were cooled to −120°C, then warmed at a rate of 4 to 10°C per minute. Measurements included the temperature at which the first liquid formed in the frozen inclusion (eutectic temperature = T_e), and the temperature of final ice disappearance (T_{mI}). Inclusions were also sequentially heated and then immediately frozen. Many inclusions more than 50 μm long burst when quickly heated to a high temperature. Therefore, the temperature of halite disappearance (T_s), of vapor (T_h *L–V* (*V*)) and liquid (T_h *L–V*(*L*)) disappearance were always measured on heating the inclusions at a rate of 1 to 5°C per minute up to 250°C, then at a rate of 0.5 to 1°C per minute above 250°C. About 80% of the measurements were duplicated to characterize and recognize leaking and stretching problems (*e.g.*, Roedder 1981; see Appendix). Measurements of some liquid-filled inclusions were repeated after storage at room temperature for 3 to 12 months. Reproducibility was always within the limit of experimental error, and inclusion morphologies were apparently unchanged. The precision of the phase-change temperatures are: ±0.2°C for T_{mI}, ± 2°C for both T_h *L–V* (*L*) and T_s. The precision of T_h *L–V* (*V*) is probably no better than 20°C because of the difficulty in observing the presence of very small amounts of liquid in gas-filled inclusions.

CO_2, CH_4, H_2S, N_2 and SO_2 were looked for in the vapor phase of all inclusion types using a M.O.L.E. Raman microprobe (Delhaye & Dhamelincourt 1975, Dhamelincourt *et al.* 1979). However, these species were all below the detection level of ≈0.5 mole %.

Description of the Anhydrite and Inclusions

Most anhydrite crystals are platy and euhedral with {001} cleavages. Many crystals have depressions, up to 20 μm wide on their surfaces. Anhydrite contains opaque inclusions of hematite from the sediments or, more typically, sector-zoned inclusions of fine-grained (≈5 μm wide) euhedral sulfides or oxides (Figs. 3a,c). In the latter case, crystals may display a bow-tie structure (see Fig. 11a of Oudin *et al.* 1984). Inclusions of magnetite, pyrrhotite, isocubanite, chalcopyrite and pyrite were identified in epigenetic anhydrite from level 1085, using reflected-light microscopy and scanning electron microscopy.

Fluid inclusions are uniformly distributed throughout the anhydrite but cannot be observed where opaque inclusions are too abundant. Most inclusions are parallel with the *c* axis of the crystal. Fluid inclusions in anhydrite are either monophase and filled with a liquid (type *L*), or are two-phase and either liquid-dominant (type *L*) or vapor-dominant (type *V*), or three-phase, *i.e.*, filled with liquid, vapor and a halite cube (type *S*). Most type-*L*, and all type-*V* and -*S* inclusions are randomly distributed, and therefore grew simultaneously with the host anhydrite as primary inclusions (*cf.* Roedder 1976). Less than 10% of type-*L* inclusions appear to be secondary; these are concentrated along ≈200-μm-long fractures. All anhydrite crystals contain type-*L* inclusions, and about two thirds contain liquid + vapor-filled aqueous inclusions and no type-*S* inclusions. One third of the crystals contains both NaCl-undersaturated and NaCl-saturated inclusions. No crystals in which all the inclusions are NaCl-saturated were observed.

Type-*L* and type-*V* inclusions differ in morphologies and distributions from type-*S* inclusions. Type-*S* inclusions are in overgrowths a few hundred μm wide at the periphery of the crystals, but are never in the cores (Fig. 3a). In contrast, type-*L* inclusions, some of which are associated with type-*V* inclusions (Fig. 3e), are characteristically in the cores of crystals (Fig. 3a). Type-*S* inclusions typically are rectangular with sharp angles, about 20 μm long and 5 μm wide (Figs. 3a,f). Type-*L* and type-*V* inclusions often have round ends, and vary from 50 μm to a few mm in length and from 1 to 15 μm in width (Figs. 3b,c,d). Type-*S* inclusions never contain opaque solids. Type-*L* and *V* inclusions can contain one or more opaque minerals. Most commonly, such opaque inclusions are at one end of the elongate inclusions (Figs. 3c,d).

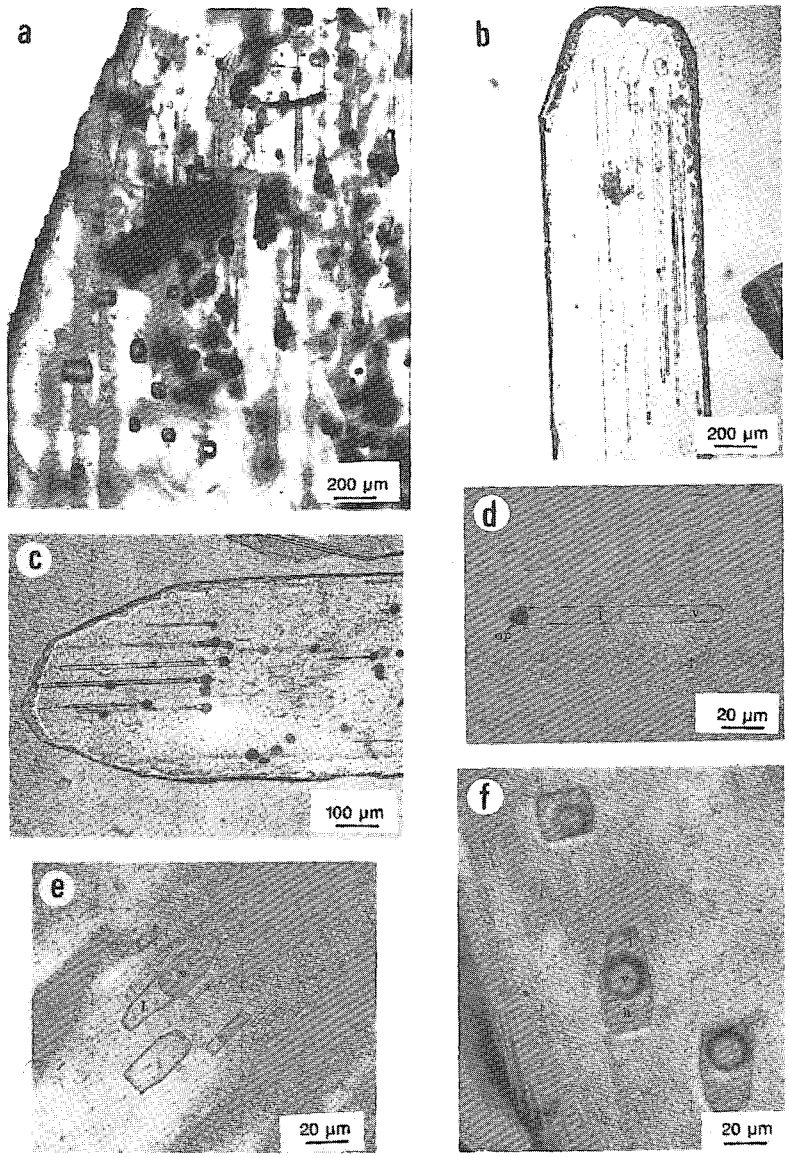

FIG. 3. Photomicrographs of fluid inclusions in anhydrite from level 1085 cm in core 268 KS. (a) Part of a polygenic anhydrite crystal with numerous opaque inclusions (oxides and sulfides) and associated tubular two-phase inclusions (liquid-dominant and vapor-dominant) in its core; isometric NaCl-saturated inclusions are trapped in crystal overgrowth. (b) Slender tubular two-phase liquid-dominant inclusion containing a liquid (*L*), a vapor (*V*) and an opaque phase (op). (c) Primary tubular two-phase inclusions initiated by opaque inclusions. (d) Three-phase type-*L* inclusion containing a liquid (*L*), a vapor (*V*) and an opaque phase (op). (e) Primary cogenetic fluid inclusions showing various liquid-to-vapor ratios as evidence of boiling. The inclusion at the upper right is vapor-filled, and the one at the bottom left is empty. (f) Primary type-*S* inclusions in an overgrowth zone of anhydrite (same legend as Fig. 3d). Note the characteristic isometric shape of inclusions. The inclusion at the bottom right is metastable as indicated by the lack of halite nucleation.

Opaque inclusions have acted as defects which have initiated the vacancies favorable for the trapping of fluid. Crystal growth has been parallel to the long axis of the inclusion and away from the opaque inclusions. In particular, crystals with a bow-tie distribution of opaque solid inclusions grew symmetrically from the center. Fine-grained hematite is less commonly trapped with the fluid in 30-μm-long type-*L* inclusions. Most type-*S* inclusions contain constant liquid:vapor ratios over a scale of a few hundred square μm. In contrast, many adjacent type-*L* and *V* inclusions have different degrees of liquid:vapor filling (ratio of liquid vol. to total vol.; Fig. 3e). Portions of anhydrite crystals can contain only type-*L* inclusions with variable degrees of filling in the range of 0.10 to 0.40 (*i.e.*, primary azonal fluid inclusions; Sobolev & Kostyuk 1975). Type-*L* inclusions underlining a growth zone in the anhydrite are uncommon; in the latter case, they are homogeneously filled and yield very constant microthermometric data (primary zonal fluid inclusions; Sobolev & Kostyuk 1975).

Most fluid inclusions in the clearer parts of the crystals have the regular shape described above and show no evidence for necking or re-equilibration. However, fluid inclusions of variable size and irregular shape can occur in the outer parts of crystals, and some of these show evidence of necking. All analytical data presented below are for inclusions with a regular shape in clear sections of anhydrite crystals.

Metastability

Many monophase, two-phase and three-phase inclusions exhibited metastable behavior in the range

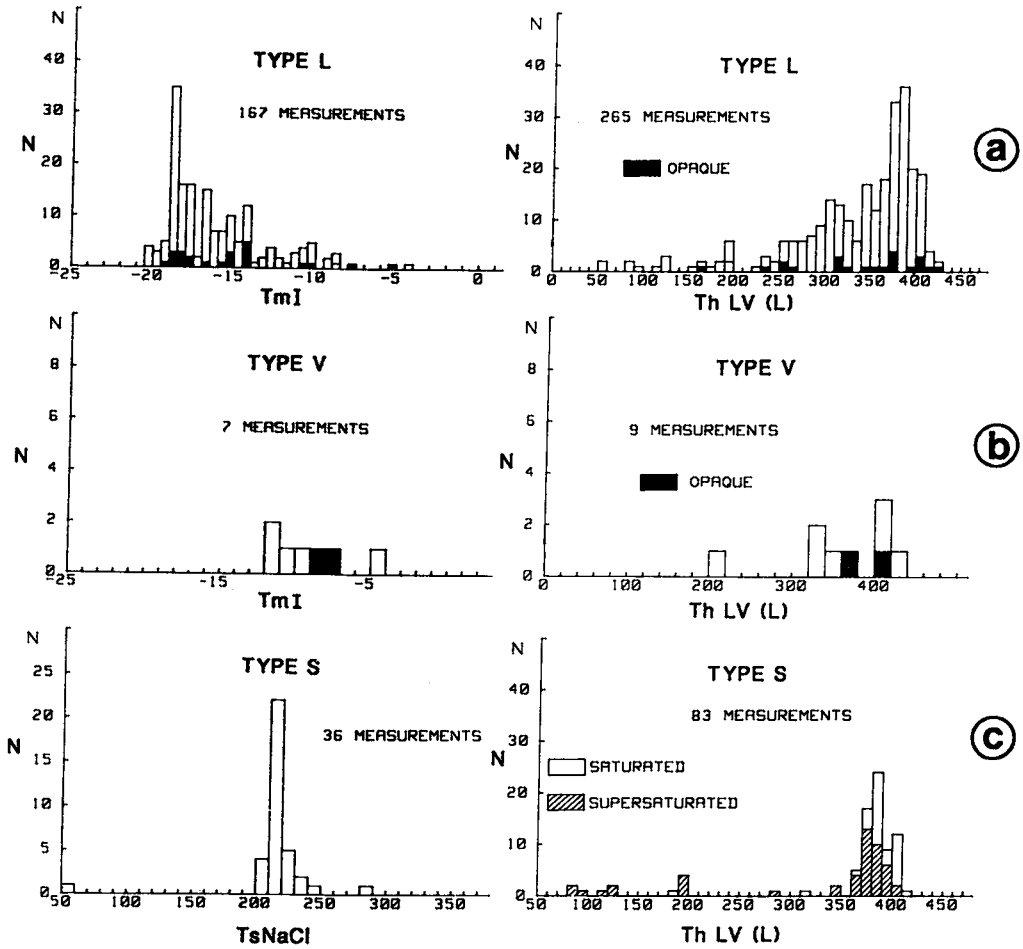

FIG. 4. Histograms of the microthermometric measurements (°C) obtained on 16 anhydrite crystals from level 1085 cm. (a) Type-*L*, (b) type-*V* and (c) type-*S* inclusions. T_{mI}: melting point of ice; T_h *LV*: homogenization temperature (*L*: to liquid; *V*: to vapor); T_sNaCl: temperature of disappearance of halite. *N*: number of measurements.

-120 to $+550$°C. In most monophase liquid-filled inclusions distributed among two-phase inclusions, a vapor bubble nucleated on cooling. Conversely, some type-*L* inclusions did not nucleate a vapor bubble on cooling after homogenization. Some primary two-phase inclusions (filled with a liquid and either a vapor or a halite cube), located among saturated three-phase inclusions, showed metastable behavior and nucleated a gas or a halite cube on abrupt cooling (Fig. 3f). Some two-phase liquid + vapor-filled inclusions were supersaturated: they contained hydrohalite at low temperatures and never nucleated halite in the course of normal cooling–heating cycles. During warming of frozen type-*V* and *L* inclusions, the first drop of liquid appeared at around -21°C, and reproducible melting points of ice were measured. Liquid-dominant two-phase inclusions, however, also exhibited a metastable behavior during low-temperature runs. Highly birefringent yellow, green, and uncolored salt hydrates were randomly formed. Up to three distinct salt-hydrates were seen to melt successively in a given inclusion. These salt-hydrates have not been identified.

Analytical Data

The microthermometric data obtained mainly on primary type-*L*, *V* and *S* inclusions are shown in Figure 4.

Type-L inclusions. At room temperature, these contain a liquid occupying at least 50% of the inclusion volume. Frequency distribution of the melting points of ice (T_{mI}) and homogenization temperatures ($T_hLV(L)$) are skewed. T_{mI} values are between -4.4 and -20.4°C, with a marked mode of -18.5°C. Most measurements are in the range -18.5 to -4.4°C (Fig. 4a). Inclusions homogenized to liquid between 55 and 420°C, with a mode of around 390°C. Secondary type-*L* inclusions were not studied systematically. Most such small inclusions homogenized below 100°C.

Type-V inclusions. At room temperature these contain a liquid occupying at least 50% of the inclusion volume. T_{mI} values in 7 inclusions are between -12.0 and -5.0°C, and homogenization temperatures from 9 inclusions are in the range 324 to 430°C (Fig. 4b). However, due to the difficulty in observing the disappearance of the vapor bubble, the precision of the homogenization measurements is very poor.

Type-S inclusions. At room temperature these contain a halite cube, liquid and vapor. All but one of the 36 inclusions analyzed contained a halite cube occupying about 30 to 40% of the inclusion and yielded T_s values in the range 201 to 283°C. Supersaturated type-*S* inclusions contain no NaCl cube, but nucleated hydrohalite on cooling. One initially supersaturated inclusion nucleated a small halite cube which dissolved at 50°C. Saturated and supersaturated type-*S* inclusions always homogenized to liquid through disappearance of the vapor bubble. Homogenization temperatures for saturated inclusions are in the range 185 to 415°C, with most values above 340°C (Fig. 4c). T_h values in supersaturated inclusions are in the range 84 to 404°C, with a larger number of lower temperatures than for NaCl-saturated inclusions (Fig. 4c).

Table 1 : Reconstructed hydrostatic pressure regime over the anhydrite veins in core 268 KS, level 1085cm. Data on Red Sea water and brines are from Brewer et al. (1969) and Hartmann (1980). Data on the core are from Thisse (1982). Fluid densities are calculated after Pitzer et al. (1984).

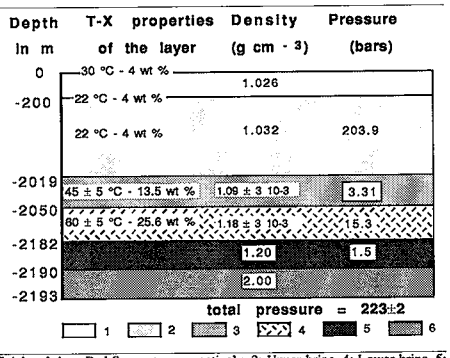

1 and 2: Surficial and deep Red Sea water, respectively. 3: Upper brine. 4: Lower brine. 5: Shaly sediment. 6: Hematite sediment.

The H_2O–NaCl System as an Analog

The fluids in primary and secondary inclusions in anhydrite are complex Na–Ca–Fe–Zn...–Cl–SO_4 brines, because the fluids are saturated with respect to $CaSO_4$ and precipitated oxides and sulfides. Numerous salt-hydrates nucleated in type-*L* inclusions during low-temperature "cycling" experiments. NaCl is certainly the dominant salt in solution. The first drop of liquid always appeared close to the eutectic point of the system H_2O–NaCl (-20.8°C; Potter *et al.* 1978). A halite cube formed in some supersaturated inclusions. The lower brine, which is representative of the hydrothermal brine, contains $\approx$15.6 wt.% Na^+ and only 0.5 wt.% Ca^{2+} and 80 ppm Fe^{2+} (Brewer *et al.* 1969, Hartmann 1985). T_{mI} values in type-*L* and *V* inclusions therefore were interpreted in terms of equiv. NaCl content (Potter *et al.* 1978). The dissolution of halite was determined from the data by Potter *et al.* (1977). Two-phase field boundaries for the H_2O–NaCl system are from the experimental studies of Khaibullin & Borisov (1966) and Parisod & Plattner (1981). Molar volumes are from Khaibullin & Borisov (1966) along the two-phase boundaries, and from Zhang & Frantz (1987) and Pitzer *et al.* (1984) in the liquid stability field.

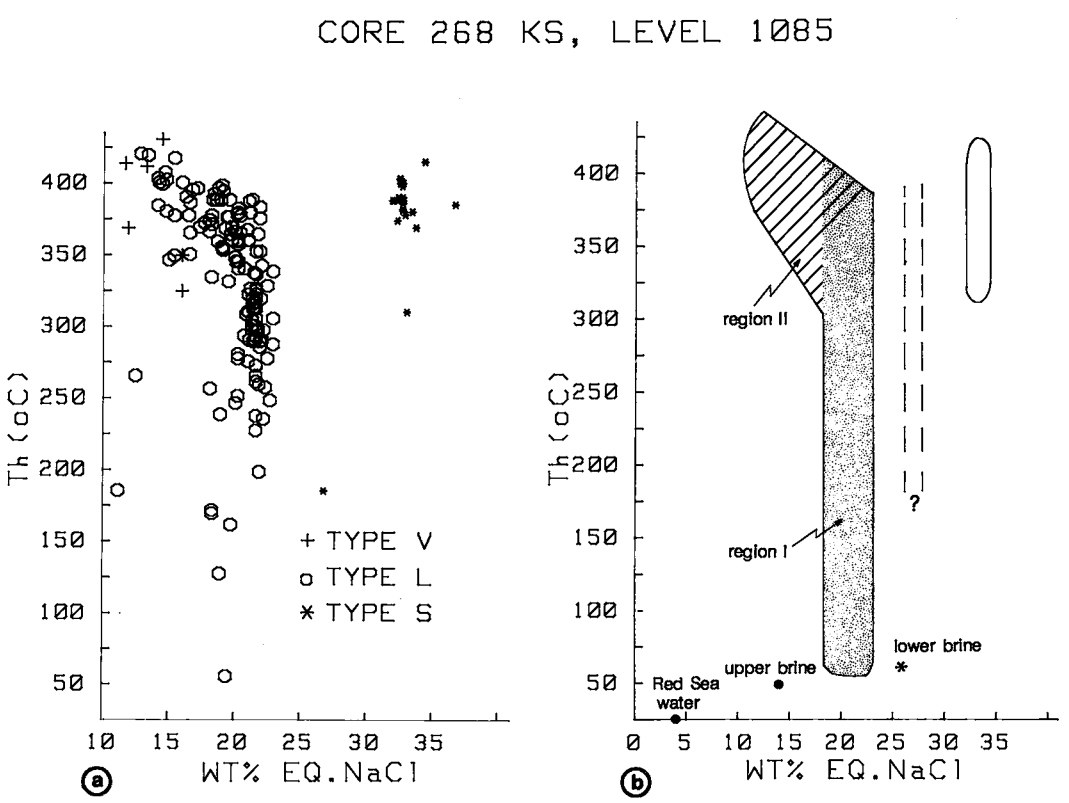

FIG. 5. (a) Homogenization temperatures for type-*L* and *S* inclusions as a function of salt content; X_w in wt.% equiv. NaCl, after Potter *et al.* 1977, 1978; (182 inclusions from 16 crystals). (b) Summary of T_h–X_w data: all the type-*L* and *V* inclusions with X_w <23 wt.% equiv. NaCl are grouped in two distinct regions, the limits of which become unclear at high temperature. The projected field of type-*S* inclusions is shown on the right; the hatched lines mark the projected field inferred for supersaturated inclusions (see text).

PRESSURE CONDITIONS IN THE SEDIMENT

The sediments in the Deep are unconsolidated muds which are occasionally indurated due to hydrothermal metamorphism (Bäcker & Richter 1973). The SW Basin sediments are crosscut by numerous sulfate and sulfide-bearing veinlets, indicating that they are consolidated enough to fracture. It is unlikely, however, that the strength of such a sediment has exceeded one bar. Fluids in Atlantis II Deep anhydrite were therefore probably trapped under hydrostatic pressure conditions.

Microfaunal studies of Red Sea sediments show that the level of the Red Sea has not varied significantly since the beginning of the Holocene (Bourdillon & Gideiri 1983). As hydrothermal processes in the SW Basin of the Deep are no older than the Holocene (Bäcker & Richter 1973), this is the maximum age of the crystals. The hydrostatic pressure at which the fluids have been trapped in anhydrite can be estimated at 223 ± 2 bars, taking into account the present column of water and sediments over the veins. The main cause of error in pressure determination arises from the fact that the temperature, and hence the density, of the lower and upper brines at the time a crystal formed is unknown (Table 1).

Data on geothermal systems show that brines can be superheated, *i.e.*, they can exist at a temperature in excess of the boiling temperature at the pressure considered (Elder 1981). This results from the metastable suppression of vapor nucleation. It cannot be excluded, therefore, that the crystals have trapped small amounts of superheated brine. The fluid inclusions therefore may indicate a minimum trapping pressure exceeding by a few bars the hydrostatic value.

INTERPRETATION OF FLUID-INCLUSION DATA

Figure 5a shows homogenization temperatures *versus* salt content for 182 type-*L*, *V* and *S* inclu-

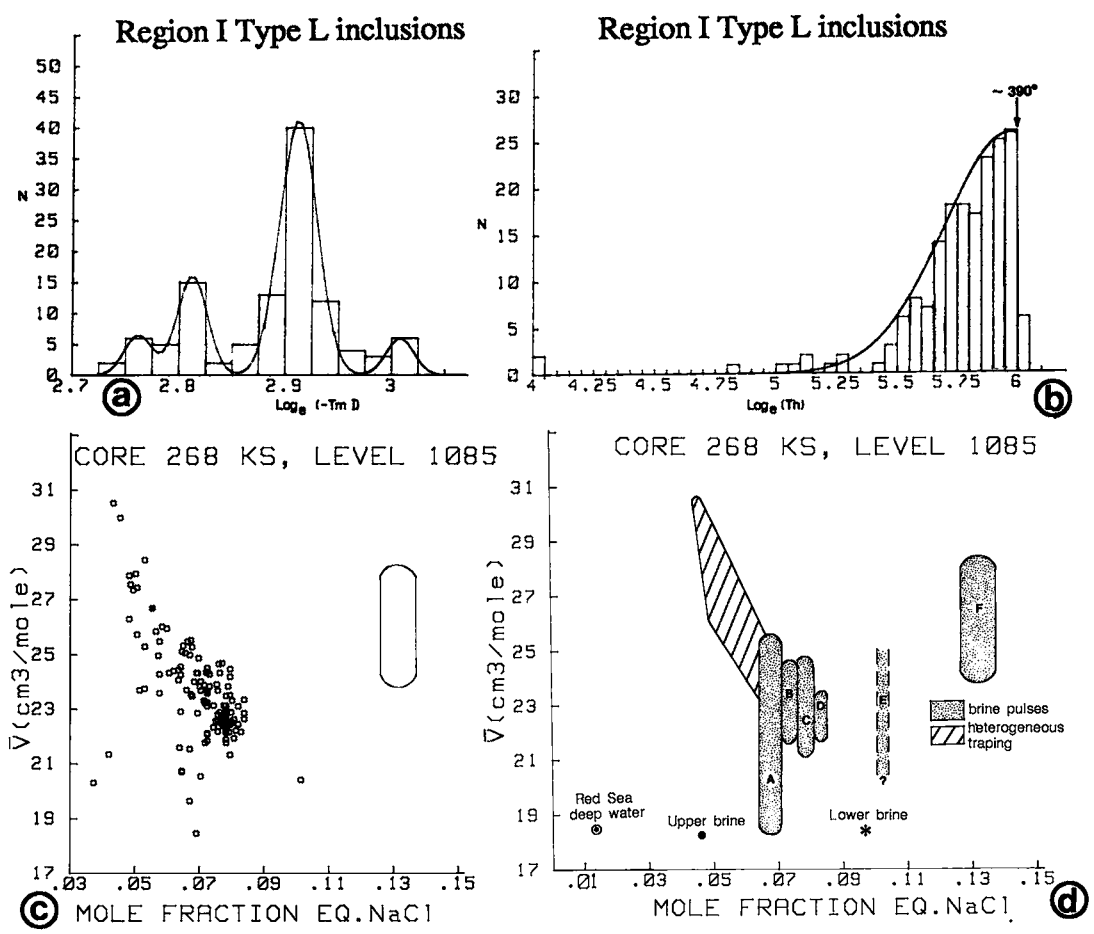

FIG. 6. Region-I type-*L* inclusions. (a): Interpreted histogram of the T_{mI} values in terms of four populations with lognormal distribution. (b) Discontinuous distribution of the T_h values, which approximates twice a lognormal law below ≈390°C, and zero above 390°C. (c) Variations of the molar volume ($\overline{V}$) of all type-*L* inclusions as a function of mole fraction equiv. NaCl (derived from the T_{mI} values as in Fig. 5; 176 inclusions from 16 crystals). The molar volumes of type-*L* inclusions are calculated using a fit of the $\overline{V}$-*T*-X experimental data for the two-phase field boundaries in the H_2O-NaCl system of Khaibullin & Borisov (1966; regression program by M. Danis, C.R.P.G.). The field of type-*S* inclusions is approximated based on experimental data of Gehrig *et al.* (1983). (d) Summary of $\overline{V}$-*X* relations. Dotted elongate area: constant composition – variable volume trends corresponding to brine pulses injected at decreasing temperatures on the seafloor and evolving without mixing, in particular with the lower brine (A to D: pulses corresponding to the four populations in Region-I type-*L* inclusions; Fig. 6a); E: projection field inferred for supersaturated inclusions, see text; F: pulse defined by type-*S* inclusions. Hatched area: inclusions resulting from *L*/*V* heterogeneous trapping (see also Fig. 9).

sions. On the T_h–X_w plane, type-*L* and *V* inclusion fluids plot on a linear trend distinct from type-*S* inclusion fluids. The magnitude of the salinity gap separating type-*L* and *V* inclusions from type-*S* inclusions is exaggerated due to metastability, as mentioned previously. Halite fails to nucleate at low temperatures from inclusion fluids with a salinity close to saturation at 25°C, *i.e.* ≈23 wt.% NaCl (*cf.* Yajima & Touray 1967). Although only one NaCl-saturated inclusion yielded a salinity of 27 wt.% equiv. NaCl, it is likely that numerous inclusions exhibiting metastable behavior have similar salinities. On Figure 5b, type-*S* inclusions with metastable behavior are therefore shown on a roughly vertical trend centered about 27 wt.% NaCl.

The region within which type-*L* and *V* inclusions plot can be subdivided into two parts (Fig. 5b). Type-*L* inclusions of 18–23 % salinity outline a vertical

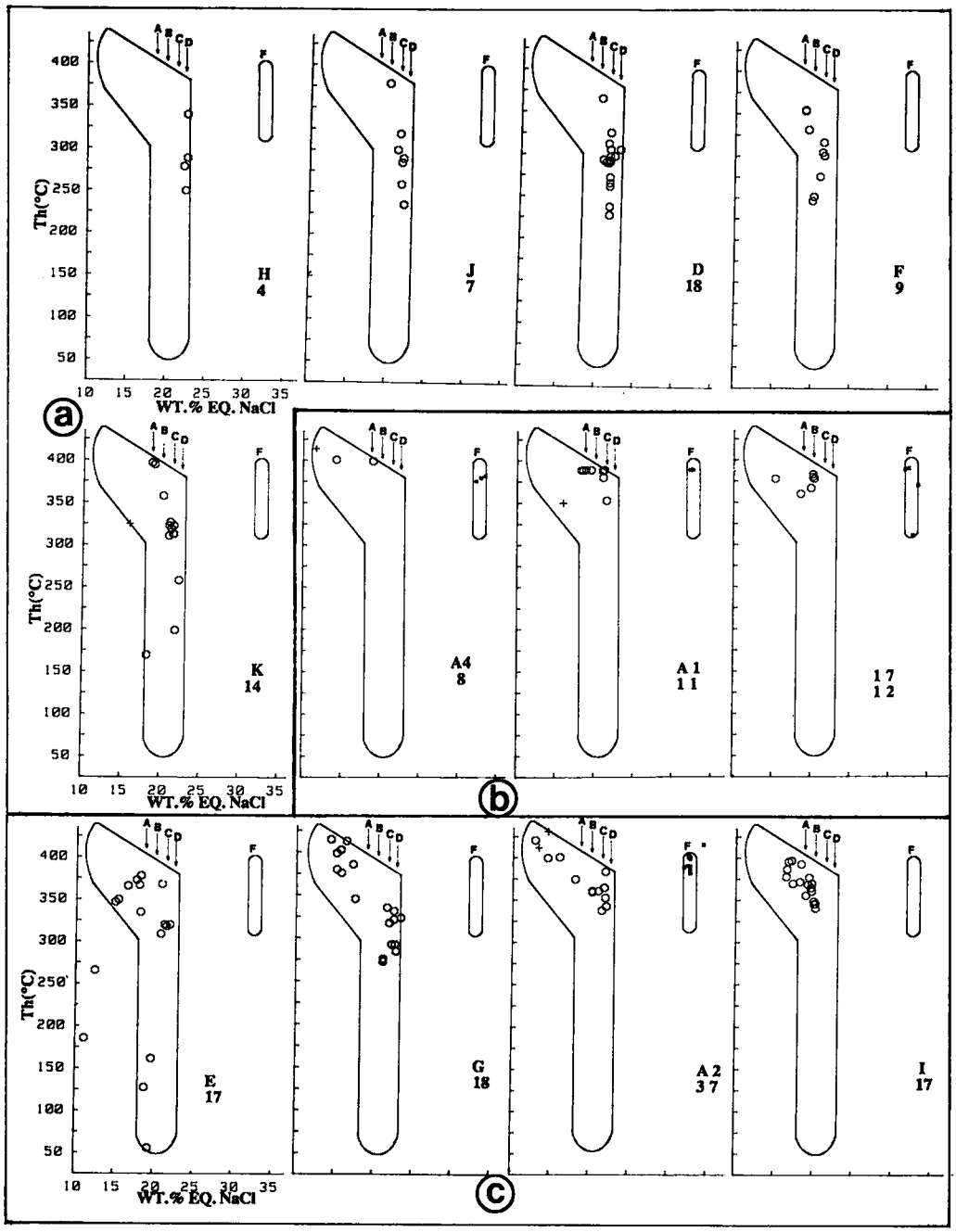

FIG. 7. T_h–X_w plot of inclusions measured in individual anhydrite crystals (the name of the crystal and the number of data points are indicated in the lower right). Type-*L* and *S* inclusions define three main fluid-inclusion patterns: (a) isochemical cooling; (b) isochemical isothermal process; (c) overprint of heterogeneous trapping on the previous patterns (see text). Numbers 1 to 6 are individual inclusions discussed in the text (Table 2). A to D and F are the brine pulses identified in Figure 6d.

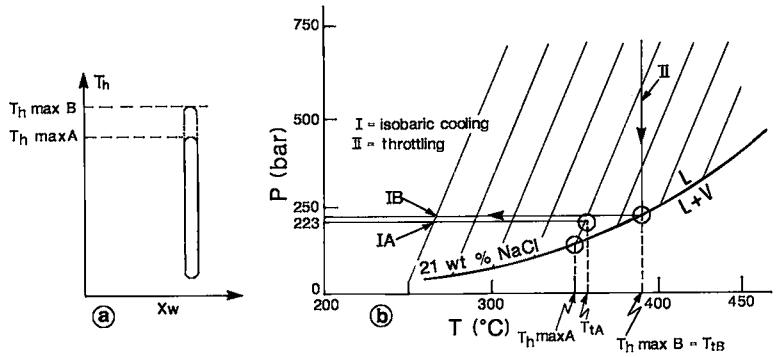

FIG. 8. Brine influxes on the seafloor under conditions of boiling (path IA) and non-boiling (path IB). (a) Schematic microthermometric signature on a T_h–X_w plot. (b) Interpreted P–T trapping conditions of a 21 wt.% NaCl brine pulse venting on the seafloor at $P = 223$ bars (after Parisod & Plattner 1981). Brine venting in an unconsolidated sediment is necessarily isobaric (path I), which excludes throttling (path II). T_t A and T_t B are the trapping temperatures of the brine, in the liquid field and under boiling conditions, respectively.

trend (region I) parallel to that defined by saturated and supersaturated inclusions. Region II includes type-V and the less saline type-L inclusions. Two distinct processes are recorded by region-I and region-II inclusions, which are discussed separately hereafter.

On Figure 5b, all type-L inclusions with $18 < X_w < 23$ wt.% are grouped in a single population. However, the histogram of the T_{mI} values of region-I type-L inclusions consists of four populations with a lognormal distribution (Fig. 6a). In contrast, the T_h values of these inclusions present a unimodal distribution, with very few values higher than the mode ≈ 390°C (Fig. 6b). Figure 6c shows that a larger scatter exists for all region-I inclusions in a $\bar{V}$–X plot compared to a T_h–X_w plot. Four vertical trends are outlined in the $\bar{V}$–X plot (trends IA to ID, Fig. 6d) which are parallel to those marked by saturated and supersaturated inclusions (trends IE and IF, Fig. 6d). These are equivalent to the four populations of inclusions identified within region-I type-L inclusions based on the T_{mI} values (Fig. 6a). Trends A to F are vertical. It therefore implies that each brine pulse underwent cooling and did not mix on the seafloor, in particular with the lower brine (Fig. 6d). Individual anhydrite crystals in fact contain type-L inclusions with a restricted salinity range. They yield the vertical T_h–X_w trends identified on the basis of the statistical analysis of all inclusions from 16 crystals (Fig. 7a). In conclusion, the trends shown in Figure 6d indicate that brine pulses progressively enriched in salts were injected intermittently at the bottom of Atlantis II Deep and cooled without mixing.

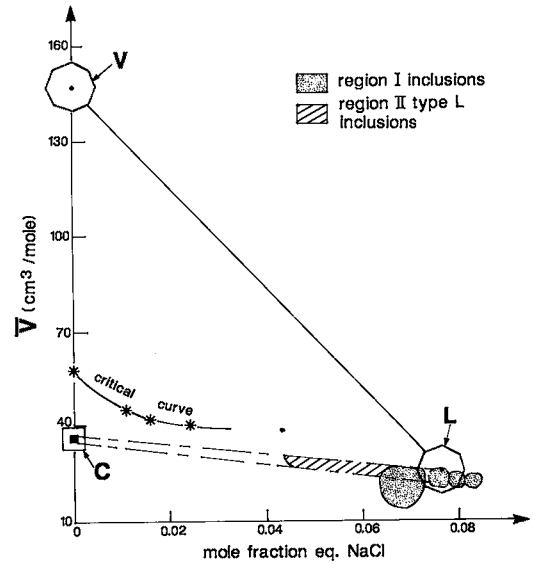

FIG. 9. Interpretative diagram showing properties of inclusions resulting from L/V heterogeneous trapping. The hexagons represent coexisting liquid (L) and vapor (V) in the H_2O–NaCl system at 390°C and 223 bars (conditions fixed by inclusion 3, Table 2, and Fig. 10; data of Khaibullin & Borisov 1966). Mechanical mixtures of these phases will plot on a straight line. Region-II type-L inclusions (hatched area) probably represent mixtures of the cooled liquid and a cooled and/or condensed vapor (point C). Region-II inclusions are close to the critical curve of the H_2O–NaCl system. Critical curve after Keenan *et al.* (1969) and Khaibullin & Borisov (1966).

It is possible to determine the P–T conditions of trapping on the seafloor for inclusions with a vertical T_h–X_w trent at ≈ 21 wt.% equiv. NaCl at a hydrostatic pressure of 223 bars (Fig. 8a). Figure 8b shows that, at P = 223 bars, the maximum homogenization temperatures for inclusions of a given composition are fixed by the temperature of the two-phase boundary (Bischoff *et al.* 1986). A 21 wt.% NaCl solution undergoes phase separation at ≈390°C, close to maximum values recorded by inclusions of that composition in anhydrite in level 1085 cm (Fig. 5a).

Region II contains type-L and V inclusions with salinities ≈ <19 wt.% equiv. NaCl. T_h values negatively correlate with salt contents (Fig. 5a). This trend is obvious in some individual crystals (Fig. 7c). Such a pattern is expected to characterize H_2O–NaCl inclusions which have trapped mechanical mixtures of immiscible liquid and vapor (*e.g.*, Ramboz *et al.* 1982, Ramboz 1983). On a $\overline{V}$–X projection, the nearly pure H_2O vapor (point V) and the 21 wt.% NaCl brine (point L) coexisting at 390°C and 223 bars have been plotted (Fig. 9). The straight line (L–V) represents mechanical mixtures of the pure end-member phases. This plot shows that region-II inclusions cannot contain mixtures of the pure end-members, as they plot markedly below line L–V. More likely, region-II inclusions contain mechanical mixtures of liquid L with a cooled condensed vapor at point C (Fig. 9). All type-V inclusions have salinities >10 wt.% equiv. NaCl, which are far in excess of the salinity of the pure unmixed vapor at about 390°C and 223 bars (≈ 0.5 wt.% NaCl; Khaibullin & Borisov 1966, Pitzer & Pabalan 1986). Therefore, all type-V inclusions are interpreted to have trapped a vapor and a significant fraction of brine. Some region-II, type-L inclusions have both salinities and T_h values comparable to those of vapor-rich inclusions (Fig. 5a). Liquid-rich and vapor-rich inclusions plotting in the same portions of the T_h–X_w plot must necessarily have been trapped at near-critical $\overline{V}$–X conditions. The mixing line L–C in fact is close to the critical curve of of the H_2O–NaCl system (Fig. 9).

Figure 10a is a $\overline{V}$–X_w plot showing the five major "isochemical cooling" trends identified in Figure 6. The maximum T_h in each trend has been outlined (points 1 to 5). Table 2 lists microthermometric data and interpreted composition–volume parameters of these five inclusions. Figure 10b shows the locations of these inclusions on a P–X projection in the H_2O–NaCl system as well as liquid + vapor–liquid boundaries at 380, 400 and 420°C (from Parisod & Plattner 1981). Within the error limits of the field boundaries and microthermometric measurements, the minimum trapping pressures of inclusions 3 and

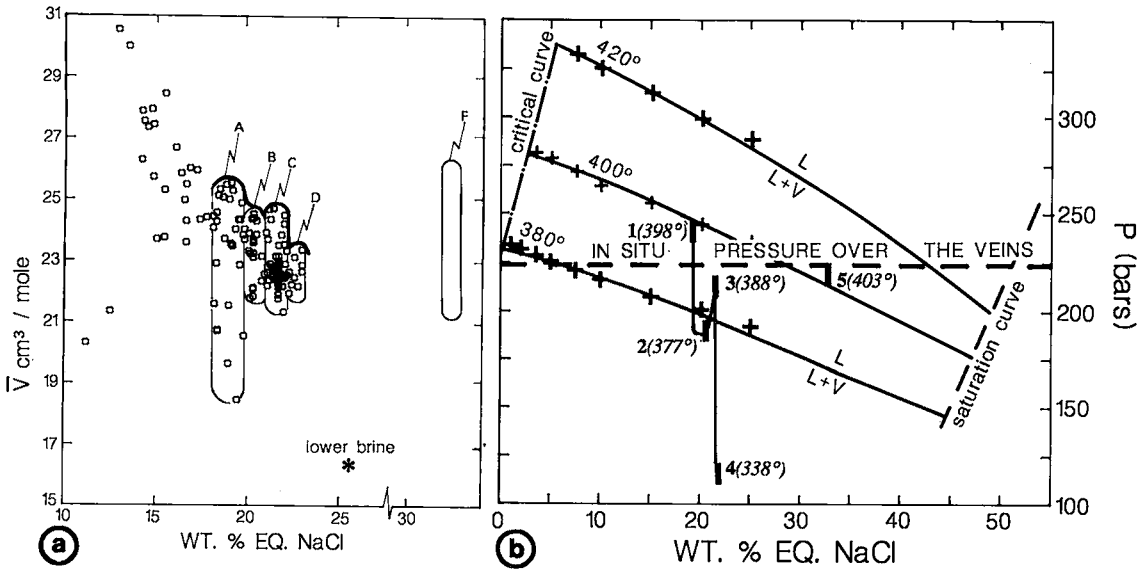

FIG. 10. Estimated P–T–X conditions of boiling at the bottom of the Atlantis II Deep. (a) $\overline{V}$–X_w plot of the type-L, V and S inclusions with superimposed trends inferred for brine pulses (Fig. 6d). The highest $\overline{V}$ in each trend is outlined (inclusions 1 to 5). (b) Comparison of the minimum trapping pressure of inclusions 1 to 5 (*i.e.*, the internal pressure at T_h) with the *in situ* pressure at the bottom of the Deep (Table 1). Microthermometric data for inclusions 1 to 5 are given in Table 2. Two-phase boundaries at 380, 400 and 420°C after Parisod & Plattner 1981, experimental points from Khaibullin & Borisov (1966). Critical and saturation curves after Keenan *et al.* (1969), Bischoff & Rosenbauer (1984), and Chou (1987).

Table 2 : Microthermometric data and interpreted composition, volume and trapping temperature of the six inclusions shown in Figure 10a (sources of experimental data as in Fig. 10).

No	TmI (°C) (±0.2)	Ts (°C) (±2)	Th(°C) (±2)	XNaCl wt%	$\bar{V}$ (cm^3/mol)	Trapping temperature (°C) at 223 bars
1	-15.3	-	398	19.04	25.6	-[a]
2	-17	-	377	20.43	24.3	379[c]
3	-18.2	-	388	21.35	24.7	388[b]
4	-20.4	-	338	22.94	23.4	345[c]
5	-	213	403	32.56.	25.6[d]	403[b]
6	-15.8	-	55	19.4	18.5[e]	64[e], 69[e]

a: inclusion resulting from heterogeneous L/V trapping; b : inclusion fluid on the two-phase field boundary at 223 bars; c : pressure correction after Zhang & Frantz (1987); d : after Gehrig et al. (1983); e : after Pitzer et al.(1984).

5 are compatible with the calculated *in situ* pressure. Brine pulses with compositions of 21.3 and 32.6 wt.% equiv. NaCl were undergoing phase separation on venting in the Atlantis II Deep sediment. By contrast, inclusions 2 and 4, respectively, plot 30 and 100 bars below the pressure of 223 bars. Microthermometric data for the remainder of the crystal which hosts inclusion 2 (crystal I, Fig. 7c) suggest heterogeneous trapping, implying boiling. Type-*L* inclusion 4 has the highest salinity, ≈23 wt.% equiv. NaCl. The latter brine pulse was recorded only in crystal H (Fig. 7a); therefore, the data required to prove boiling for that pulse are insufficient. Inclusion-1 fluid plots 18 bars above the calculated *in situ* pressure for the anhydrite veins. This probably implies that this inclusion contains a mechanical mixture of liquid and vapor (Ramboz 1983), consistent with its location close to the "heterogeneous trapping" trend (Figs. 5,6).

Discussion

Boiling on and below the seafloor has long been invoked in the formation of certain ancient base metal deposits (Ridge 1973, Finlow-Bates & Large 1978, Spooner 1980, Anderson 1983). Fluids of variable salinities in present-day active subaerial geothermal systems are known to result from different degrees of boiling at depth (*e.g.*, Fournier 1981). Fluids enriched or depleted in chlorine relative to seawater circulate in the oceanic crust (Jehl *et al.* 1977, Vanko 1984, Dubois 1984, Dubois *et al.* 1984), or are discharged at vents or trapped in hydrothermal minerals (or both) on 23°N EPR (Cosens Gallinatti 1984), 21°N EPR (Le Bel & Oudin 1982, Von Damm *et al.* 1985), 13°N EPR (Michard *et al.* 1984), and on the Southern Juan de Fuca Ridge (Bischoff & Pitzer 1985). However, the Cl content of the fluid alone does not provide any definite indication of boiling on or near the seafloor, as it is partly controlled by hydration processes and the formation of Fe hydroxychlorides during basalt–seawater interaction (Seyfried *et al.* 1986). Liquid-rich and vapor-rich inclusions coexisting in the same mineral seldom have been reported in oceanic settings (*e.g.*, Spooner 1980).

Fluid-inclusion data from Atlantis II Deep anhydrite provide direct evidence for boiling near the seafloor in the SW Basin. The data therefore support previous conclusions, based on hydrological observations, that hydrothermal discharge in the Atlantis II Deep, being accomplished by a vapor phase, is of a geyser type (Ross 1972, Schoell & Hartmann 1978). Complementary geochemical studies on core 268 KS have shown that gold precipitates ≈1 m above the boiling zone (Oudin 1987). The history of the brines can be reconstructed as follows (Fig. 11). As boiling of the ≈19 wt.% equiv. NaCl fluid proceeded at depth, liquids progressively enriched in salt ascended towards the seafloor under the *P–T* conditions defined by boiling curves. Data from type-*L* and *S* inclusions suggest that these liquids were separated from initially coexisting vapor (open-system boiling) and were injected intermittently. The brine influxes in the Deep were probably controlled by tectonics.

At 21°N, EPR, it is now established that a magma chamber exists 1 to 4 km below the vents (*e.g.*, McClain *et al.* 1985), and that the hydrothermal fluid has acquired its chemical character near the top of the magma chamber at around 400°C and 400 bars (*e.g.*, Bischoff 1980, Seyfried & Janecky 1985). In contrast, the nature of the seafloor underlying the Atlantis II Deep is uncertain (Le Quentrec *et al.* 1987). The fact that hydrothermal solutions discharged at the Deep bottom have undergone long-duration boiling implies that the deep fluid reservoir has a limited volume. Besides, the near-isothermal boiling observed at surface requires a large heat supply, and hence probably a magma in the source area. The *P–T* conditions in the reservoir were, at least transiently, below critical (*i.e.*, ≈540°C and 700 bars for a 19 wt.% NaCl solution; Urusova 1974). The enthalpy of the fluid in the reservoir can be estimated to have been about 1950 J g^{-1} (Hass 1976, Bischoff & Pitzer 1985), assuming isenthalpic boiling during ascent and using the enthalpy–salinity projections of Fournier (1981).

Hedenquist & Henley (1985) suggested that "...boiling of a hydrothermal fluid flowing rapidly through a fracture may not always be preserved in fluid inclusions". The vapor resulting from fluid boiling at low pressure (P <200 bars) is in fact rarely trapped in inclusions (Ramboz *et al.* 1982, Weisbrod 1984, Aissa *et al.* 1987). In the Atlantis II geothermal system, evidence for boiling is provided by heterogeneous trapping of liquid and vapor in early-formed anhydrite. The histogram of T_h values of region-I type-*L* inclusions resulting from homogeneous trapping is skewed, with a marked discontinuity near the temperature of the boiling; the distribution equals twice a lognormal law below 390°C, and zero above 390°C (Fig. 6b). If the liquids trapped in crystals under boiling conditions are perfectly separated

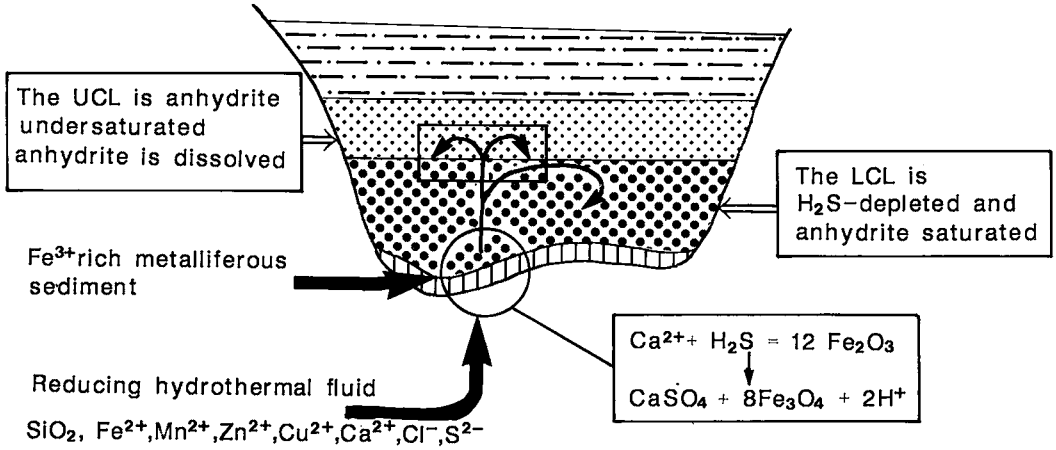

FIG. 11. Schematic representation of anhydrite deposition in Atlantis II Deep sediments as a result of redox reactions between the hydrothermal fluid and the Fe^{3+}-bearing sediment (modified after Hartmann 1973 and Cole 1983). The distribution of sulfates and sulfides in the lower (LCL) and upper (UCL) brines is also shown (after Hartmann 1985, Zierenberg & Shanks 1986, and unpublished calculations by C. Monnin).

from the vapor and there is no superheating, the probability of trapping inclusions that yield homogenization temperatures higher than the boiling temperature is zero. Boiling conditions, therefore, could have been reconstructed even in the absence of *L/V* heterogeneous trapping.

The present data allow an estimate of the minimum temperature which has prevailed in the SW Basin sediments. Inclusion 6 in Figure 10a implies a minimum trapping temperature of 69°C for the fluids in the anhydrite of level 1085 (Table 2). This temperature is 7°C higher than the maximum value measured in the Deep sediments (Erickson & Simmons 1969). However, these measurements were for depths not greater than 3 m below the seafloor, whereas the value of 69°C is for a depth of 11 m.

All salinity variations recorded by primary inclusions in anhydrite can be attributed either to variable degrees of boiling at depth, or to heterogeneous trapping. *In situ* mixing with the lower brine is unlikely as it is not supported by a relevant mixing trend (Figs. 6c,d); the linear trends of constant salinity and variable molar volumes identified in the crystals (Figs. 5,6) correspond to brine pulses undergoing "isochemical cooling". Anhydrite has a prograde solubility above 250°C in solutions with more than ≈15 wt.% NaCl (Blount & Dickson 1973), and therefore anhydrite can precipitate from a cooling, high-temperature saline solution. However, cooling is not the main mechanism in the formation of epigenetic anhydrite, as 8 of the crystals examined had a very narrow range, both in homogenization temperatures and salinity, for type-*L* inclusions in region I and type-*S* inclusions (Fig. 7b). In the growth zones of these crystals, type-*L* and *S* inclusions with homogeneous morphologies and fillings yielded well-constrained microthermometric data. Calculations at and below 350°C show that boiling does not favor anhydrite precipitation. Anhydrite is more likely to precipate last from boiling hydrothermal solutions (Drummond & Ohmoto 1985). This is in contrast to the nature of the crystals and fluid inclusions from the cores to peripheries. These suggest that, as the fluids became more saline after prolonged subseafloor boiling, they became less saturated with respect to anhydrite. Anhydrite crystals initially grew too quickly for a vapor phase to separate; the fluid was trapped in elongate tubular cavities with disequilibrium morphologies. Saline residual brines were finally trapped in 500-μm-wide crystal overgrowths.

Hydrothermal vein minerals in the SW Basin are thought to have formed mainly by precipitation from hydrothermal brines, with only limited reaction with the sediment (Hackett & Bischoff 1973, Zierenberg & Shanks 1983, Pottorf & Barnes 1983). The Fe^{2+}-bearing minerals (ilvaite and magnetite, formed after hematite: so-called "mushketovite") which precipitated around the vents, are considered to have formed by incorporation of the Fe^{2+} from the fluid, exclusive of any *in situ* reduction of ferric iron from the sediment. A careful examination of epigenetic veins in SW Basin cores shows that both magnetite and ilvaite occur in two distinct mineralogical forms (Oudin *et al.* 1984, unpubl. data). Euhedral crystals were apparently precipitated directly from the fluid, whereas poikilitic aggregates are suggestive of replacement (see Figs. 8c and 10a in Oudin *et al.* 1984).

In the SW Basin sediments, lateral mineralogical

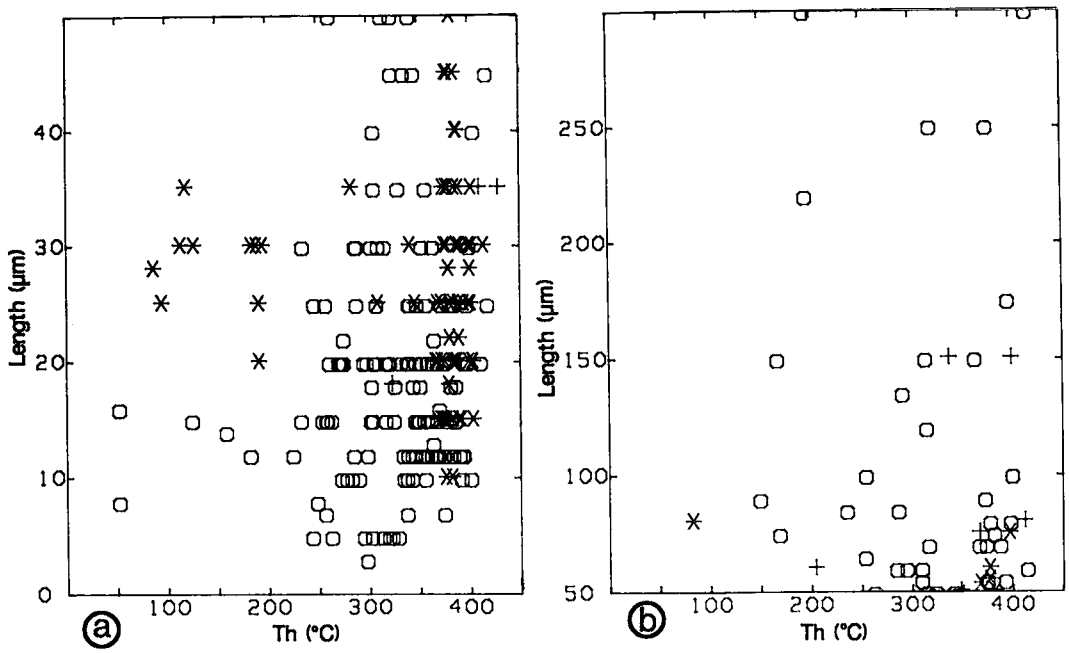

FIG. 12. Variations of homogenization temperatures (T_h) *versus* inclusion length (mm) for type-*L*, *V* and *S* inclusions (symbols as in Fig. 3). (a) 0–50-μm-long inclusions. (b) 50–350-μm-long inclusions. Symbols as in Figure 5a.

changes around the vents include: (1) the development of ferrous silicates and oxides; (2) the progressive change from dioctahedral nontronite to trioctahedral chamosite or ferroan saponite (Pottorf 1980, Zierenberg & Shanks 1983); (3) the appearance of minor ilvaite (Pottorf 1980, Oudin *et al.* 1984); (4) a progressive transition from goethite to hematite to magnetite towards the SW Basin (Bischoff 1969, Hackett & Bischoff 1973); and (5) the presence near the vents of "mushketovite" (Oudin *et al.* 1984). Badaut *et al.* (1985) also described a trioctahedral Fe^{2+}-bearing clay of a minnesotaite type associated with sulfides in the upper part of a SW Basin core, above the sulfate-enriched layer. By analogy with contact metamorphic aureoles (Thompson 1972), the bulk mineralogical changes marking the thermal metamorphism of SW Basin sediment around the vents are best explained in terms of dehydration, (de)carbonation, and/or sulfidation/sulfatation reactions. The last are initiated by the diffusion of hydrothermal H_2S through the sediment. Anhydrite and Fe^{2+}-bearing minerals with replacement textures around brine vents are probably the end products of redox reactions. An anhydrite–magnetite-forming reaction can be written as:

$$Ca^{2+} + H_2S + 12\ Fe_2O_3 \rightarrow CaSO_4 + 8\ Fe_3O_4 + 2H^+ \quad (1)$$

The formation of magnetite after hematite following that reaction implies a volume reduction by ≈25% of the solids, which can account for the porous aspect of the "mushketovite". Anhydrite formation is induced by the contrast in redox potential between the hydrothermal fluid and the sediment. Reaction (1) explains why the earlier sulfide-enriched fluid became drastically saturated with respect to anhydrite on venting through the sediment, whereas the residual, salt-enriched oxidized brine did not. Hartmann (1985) noted that, during the period of increasing hydrothermal activity from 1966 to 1977, the dissolved sulfate of the upper brine increased compared with the theoretical value based on conservative mixing of the lower brine with Red Sea water. Because more suspended sulfides were supplied to the lower brine, Hartmann (1985) proposed that the excess sulfate in the upper brine resulted from the oxidation of lower brine sulfides in the transition zone at its contact with the upper brine. Zierenberg & Shanks (1986) showed, however, that the calculated isotopic composition of the excess sulfate in the upper brine was incompatible with the latter origin, and favored the presence of particulate anhydrite in the lower brine itself. Zierenberg & Shanks (1986) therefore suggested that the excess sulfate was supplied through the interface to the upper brine and subsequently was redissolved. These latter results support our interpretation that the H_2S from the hydrothermal fluid venting in the Atlantis II Deep

was oxidized through reaction with the sediment, and now occurs as sulfate in the lower brine.

In contrast to the anhydrite crystals from level 1085 in core 268 KS, very few fluid inclusions have been observed in epigenetic anhydrite from other SW Basin cores. Epigenetic anhydrite crystals from the cores described by Zierenberg & Shanks (1983) are fibrous in comparison to the euhedral anhydrite from level 1085 (Oudin *et al.* 1984). The latter crystals contain slender fluid inclusions ($<5\mu$m), with a small to non-existent vapor bubble. The anhydrite crystals from core 268 KS are thought to be very recent for the following reasons. Core 268 KS was collected along a hydrothermally active transform fault in the SW Basin (Fig. 1c). Indeed, many authors have stated that hydrothermal activity in the Red Sea is related to transform-fault activity (Bäcker *et al.* 1975, Bignell 1975, Bertin *et al.* 1979, Pautot 1983). The episodic nature of activity inferred from the anhydrite crystals is in good agreement with the recorded recent fluctuations of the hydrothermal activity (Hartmann 1980). The average temperature of brine discharge implied by fluid inclusions in level 1085 anhydrite is consistent with that obtained from revised estimations of the exchanges of heat and mass in the Atlantis II Deep for the past 15 years (Ramboz & Danis 1987, and submitted).

Conclusions

Epigenetic anhydrite from level 1085 cm in core 268 KS has trapped liquid-rich inclusions which either contain mechanical mixtures of liquid and vapor, or result from homogeneous trapping. These are distinguished using composition–volume projections (Ramboz 1983). Anhydrite was precipitated from successive boiling brine pulses with salinities progressively increasing from 19 to 32 wt.% equiv. NaCl. The maximum homogenization temperatures of the pure liquids trapped in anhydrite are in the range 390–403°C and are compatible with boiling of the brines on the seafloor at a hydrostatic pressure fixed by the overlying water and sediment column (*i.e.*, 223 bars). This study confirms previous conclusions, based on hydrological studies, that the hydrothermal activity in the Atlantis II Deep is of a geyser type (Ross 1972, Schoell & Hartmann 1978). The vapor was already cooled and partly mixed with the coexisting liquid at the time of trapping. The present data therefore support the suggestion by Bischoff & Pitzer (1985) that the low-salinity fluids (around 1.9 wt.% NaCl) collected from differents vents at 11°–13°N, EPR, represent fluids which underwent phase separation, then cooled or mixed (or both) during ascent. Finally, the present data show that boiling of natural complex brines is best represented by liquid-rich inclusions referred to the system H_2O–NaCl (Haas 1971, Bischoff *et al.* 1986). The distribution of T_h values of type-L inclusions resulting from homogeneous trapping is diagnostic of unmixing, and the P–T boiling conditions could therefore have been reconstructed even in the absence of L/V heterogeneous trapping.

Anhydrite crystals are polygenic. (1) Crystal cores grew from less saline, sulfide-bearing fluids. During this process, mechanical mixtures of the coexisting liquid and vapor were trapped in tubular fluid inclusions with disequilibrium morphologies. (2) In contrast, later crystal growth was from the residual solutions which had boiled longer. Liquids devoid of vapor were trapped in small isometric cavities. The formation mechanism which best accounts for the contrasting nature of the crystals and their fluid inclusions from cores to peripheries is as follows. The fluid reached anhydrite saturation on venting on the seafloor because the hydrothermal sulfides were rapidly oxidized to sulfates. This reaction was coupled with the reduction of iron from Fe^{3+}-bearing oxides and silicates in the sediment. Anhydrite, like "mushketovite" and some of the ilvaite, is considered to be the product of interaction of the fluid and the sediment.

The anhydrite was probably formed recently from brines discharged at about 400°C along a ≈ 1 km length of the active transform fault which crosscuts the SW Basin (Bäcker *et al.* 1975, Cole 1983; Fig. 1c). For the past 15 years, the mass-discharge flow rate in the Atlantis II Deep has been around 278 kg s^{-1}. By comparison at 21°N, EPR, the vents along 1 km of the ridge have yielded an instantaneous outflow of 150 ± 60 kg s^{-1}, with vent temperatures ≤ 358°C (Converse *et al.* 1984).

The fact that the brines in the Atlantis II Deep discharge at higher temperature and undergo near-isothermal boiling implies that there is a fluid reservoir, with a limited volume at depth, which is heated by a magma. Maximum discharge temperatures on the seafloor are fixed by unmixing conditions. These increase with increase in pressure, or depth and salinity. Although the hydrostatic pressure is lower, the hydrothermal fluid in the Atlantis II Deep discharges at a higher temperature than the one at 21°N, because it is more than 4 times richer in salt.

Acknowledgements

We wish to thank H.E.Z. Mustapha and Z.A. Nawab, respectively Secretary General and Deputy of the Saudi Sudanese Red Sea Joint Commission, for allowing us to study the core sample. The manuscript was improved thanks to the many suggestions from F. Albarède, M. Arnold, J.J. Royer, A. Mezgache, S.M.F. Sheppard and A. Weisbrod. Constructive reviews by T.J. Barrett, R. Linnen and an anonymous referee were greatly appreciated. We thank V. Embareck, J. Gorau, and A. Legros for technical assistance in preparing the manuscript. This research received financial support from A.T.P. "Géochimie et Métallogénie 1983".

REFERENCES

AISSA, M., WEISBROD, A. & MARIGNAC, C. (1987): Caractéristiques chimiques et thermodynamiques des circulations hydrothermales du site d'Echassières. *En* Géologie Profonde de la France (M. Cuney & A. Autran, eds.). Tome **1**, 241-271.

ANDERSON, R.V. (1983): Boiling deep below the ocean. *Nature* **303**, 283.

BÄCKER, H. & RICHTER, H. (1973): Die Rezente hydrothermal-sedimentäre Lagerstätte Atlantis II-Tief im Roten Meer. *Geol. Rundschau* **3**, 697-741.

_____, LANGE, K. & RICHTER, H. (1975): Morphology of the Red Sea central graben between Subair Islands and Abul Kizzan. *Geol. Jahrb.* **13**, 79-123.

_____ & _____ (1987): Recent hydrothermal metal accumulation, products and conditions of formation. *In* Marine Minerals (P.G. Teleki *et al.*, eds.), 317-337. Reidel Publ. Co., Dordrecht, Holland.

BADAUT, D., BESSON, G., DECARREAU, A. & RAUTUREAU, R. (1985): Occurrence of a ferrous, trioctahedral smectite in recent sediments of Atlantis II Deep, Red Sea. *Clay Minerals* **20**, 389-404.

BERTIN, J., PEDEUX, J.P. & MAGENHAM, J.C. (1979): Contribution de la géophysique et de l'océanographie physique à la recherche et à l'exploration des boues métallifères de la Mer Rouge. *En* Ressources Minérales Sous-Marines. *Documents B.R.G.M.* **7**, 339-366.

BIGNELL, R.D. (1975): Timing, distribution and origin of submarine mineralization in the Red Sea. *Trans. Inst. Mining Metall.* **84**, 1-6.

BISCHOFF, J.L. (1969): Goethite-hematite stability relations with relevance to sea water and the Red Sea brine system. *In* Hot Brines and Recent Heavy Metal Deposits in the Red Sea (E.T. Degens & R.A. Ross, eds.). Springer-Verlag, Berlin, 402-406.

_____ (1980): Geothermal sytem at 21°N, East Pacific Rise: physical limits on geothermal fluid and role of adiabatic expansion. *Science* **207**, 1465-1469.

_____ & PITZER, K.S. (1985): Phase relations and adiabats in boiling seafloor geothermal systems. *Earth Planet. Sci. Lett.* **75**, 327-338.

_____ & ROSENBAUER, R.J. (1984): The critical point and two-phase boundary of seawater, 200-500°C. *Earth Planet. Sci. Lett.* **68**, 172-180.

_____, _____ & PITZER, K.S. (1986): The system H_2O–NaCl: Relations of vapor-liquid near the critical temperature of water and vapor-liquid-halite from 300° to 500°C. *Geochim. Cosmochim. Acta* **50**, 1437-1444.

BLANC, G. (1987): *Géochimie de la Fosse Atlantis II (Mer Rouge): Evolution Spatio-Temporelle et Rôle de l'hydrothermalisme.* Ph. D. thesis, Univ. Pierre et Marie Curie, Paris, France.

BLOUNT, C.W. & DICKSON, F.W. (1973): Gypsum-anhydrite equilibria in systems $CaSO_4$–H_2O and $CaSO_4$–NaCl–H_2O. *Amer. Mineral.* **58**, 323-331.

BODNAR, R.J. & BETHKE, P.M. (1984): Systematics of stretching of fluid inclusions I: Fluorite and sphalerite at 1 atmosphere confining pressure. *Econ. Geol.* **79**, 141-161.

BOURDILLON, C. & GIDEIRI, V.A. (1983): Étude micropaléontologique de deux carottes prélevées dans la fosse Atlantis II (Mer Rouge): âge de la mise en place et milieu de dépôt des boues métallifères. *C.R. Acad. Sci., Paris* **296**, 1271-1274.

BREWER, P.G. & SPENCER, D.W. (1969): A note on the chemical composition of the Red Sea brines. *In* Hot Brines and Recent Heavy Metal Deposits in the Red Sea (E.T. Degens & D.A. Ross, eds.). Springer-Verlag, Berlin, 174-179.

_____, DENSMORE, C.D., MUNNS, R. & STANLEY, R.J. (1969): Hydrography of the Red Sea brines. *In* Hot Brines and Recent Heavy Metal Deposits in the Red Sea (E.T. Degens & D.A. Ross, eds.). Springer-Verlag, Berlin, 138-147.

CHOU, I.-MING (1987): Phase relation in the system NaCl-KCl-H_2O. III: Solubilities of halite in vapor-saturated liquids above 445°C and redetermination of phase equilibrium properties to 1000°C and 1500 bars. *Geochim. Cosmochim. Acta* **51**, 1965-1975.

COLE, T.G. (1983): Oxygen isotope geothermometry and origin of smectites in the Atlantis II Deep, Red Sea. *Earth Planet. Sci. Lett.* **66**, 166-176.

CONVERSE, D.R., HOLLAND, H.D. & EDMOND, J.M. (1984): Flow rates in the axial hot springs of the East Pacific Rise (21°N): implications for the heat budget and the formation of massive sulphide deposits. *Earth Planet. Sci. Lett.* **69**, 159-175.

COSENS GALLINATTI, B. (1984): Initiation and collapse of active circulation in a hydrothermal system at the Mid-Atlantic Ridge, 23°N. *J. Geophys. Res.* **89**, 3275-3289.

CRAIG, H. (1969): Geochemistry and origin of the Red Sea brines. *In* Hot Brines and Recent Heavy Metal Deposits in the Red Sea (E.T. Degens & R.A. Ross, eds.). Springer-Verlag, Berlin, 208-242.

DELHAYE, M. & DHAMELINCOURT, P. (1975): Raman microprobe and microscope laser excitation. *J. Raman Spectrosc.* **3**, 33-43.

DHAMELINCOURT, P., BÉNY, J.M., DUBESSY. J. & POTY, B. (1979): Analyse d'inclusions fluides à la

microsonde Mole à effet Raman. *Bull. Minéral.* **102,** 600-610.

DOUKHAN, J.C. & TRÉPIED, L. (1985): Plastic deformation of quartz single crystals. *Bull Minéral.* **108,** 97-123.

DRUMMOND, S.E. & OHMOTO, H. (1985): Chemical evolution and mineral deposition in boiling hydrothermal systems. *Econ. Geol.* **80,** 126-147.

DUBOIS, M. (1984): *Plagiogranites et Hydrothermalisme: Une Approche à Partir des Complexes Ophiolitiques de Chypre et d'Oman.* Ph.D. thesis, Univ. Nancy I, France.

_____, CHAROY, B. & ONNENSTETTER, M. (1984): The importance of fluid phases in the genesis and alteration of the ophiolitic "plagiogranites" of Cyprus and Oman. *Ofioliti* **9,** 688-689.

ELDER, J. (1981): Particular discharge mechanisms. *In* Geothermal Systems. Academic Press, London, 382-417.

ERICKSON, A.J. & SIMMONS, G. (1969): Thermal measurements in the Red Sea hot brine pools. *In* Hot Brines and Recent Heavy Metal Deposits in the Red Sea (E.T. Degens & D.A. Ross, eds.). Springer-Verlag, Berlin, 114-121.

FINLOW-BATES, T. & LARGE, D.E. (1978): Water depth as major control on the formation of submarine exhalative ore deposits. *Geol. Jahrb.* **30,** 27-30.

FOURNIER, R.O. (1981): Application of water geochemistry to geothermal exploration and reservoir engineering. *In* Geothermal Systems: Principles and Case Histories (L. Rybach & J.P. Muffler, eds.). Wiley, New York, 109-143.

GEHRIG, M., LENTZ, H. & FRANCK, E.U. (1983): Concentrated aqueous sodium chloride solutions from 200 to 600°C and to 3000 bar. Phase equilibria and PVT-data. *Ber. Bunsenges Phys. Chem.* **87,** 597-600.

GRATIER, J.P. & JENATTON, L. (1984): Deformation by solution-deposition and re-equilibration of fluid inclusions in crystals depending on temperature, internal pressure and stress. *J. Struct. Geol.* **6,** 189-200.

HAAS, J.L., JR. (1971): The effect of salinity on the maximum thermal gradient of a hydrothermal system at a hydrostatic pressure. *Econ. Geol.* **66,** 940-946.

_____ (1976): Thermodynamic properties of the coexisting phases and thermochemical properties of the NaCl component in boiling NaCl solutions. *U.S. Geol. Surv. Bull.* **1421-B.**

HACKETT, J.P., JR. & BISCHOFF, J.L. (1973): New data and the stratigraphy, extent, and geologic history of the Red Sea geothermal deposits. *Econ. Geol.* **68,** 553-564.

HARTMANN, M. (1973): Untersuchung von suspendierten Material in der Hydrothermalaugen des Atlantis II Tiefs. *Geol. Rundschau* **62,** 742-754.

_____ (1980): Atlantis II Deep geothermal brine system. Hydrographic situation in 1977 and changes since 1965. *Deep-Sea Research* **279,** 141-161.

_____ (1985): Atlantis II Deep geothermal brine system. Chemical processes between hydrothermal brines and Red Sea Deep water. *Mar. Geol.* **64,** 157-177.

HEDENQUIST, J.W. & HENLEY, R.W. (1985): The importance of CO_2 on the freezing point measurements of fluid inclusions: Evidence from active geothermal systems and implications for epithermal ore deposition. *Econ. Geol.* **80,** 1379-1406.

JEHL, V., POTY, B. & WEISBROD, A. (1977): Hydrothermal metamorphism of the oceanic crust in the North Atlantic Ocean. *Bull. Soc. Géol. franç.* **6,** 1213-1221.

KEENAN, J.H., KEYES, F.G., HILL, P.G. & MOORE, J.G. (1969): *Steam Tables.* Wiley, New York.

KHAIBULLIN, K. & BORISOV, N.M. (1966): Experimental investigation of the thermal properties of aqueous and vapor solutions of sodium and potassium chlorides at phase equilibrium. *Teplofizika Vysokikh Temperatur* **4,** 518-523. (English transl., 489-494).

KUSAKABE, M., CHIBA, H. & OHMOTO, H. (1982): Stable isotopes and fluid inclusion study of anhydrite from the East Pacific Rise at 21°N. *Geochem. J.* **16,** 89-95.

LARSON, L.T., MILLER, J.D., NADEAU, J.E. & ROEDDER, E. (1973): Source of error in low-temperature inclusion homogenization determination, and correction on published temperature for the East Tennessee and Laisvall deposits. *Econ. Geol.* **68,** 113-116.

LE BEL, L. & OUDIN, E. (1982): Fluid inclusion studies of deep-sea hydrothermal sulfide deposits on the East Pacific Rise near 21°N. *Chem. Geol.* **37,** 129-136.

LE QUENTREC, M.F., SICHLER, B. & BAYER, R. (1987): Magnétisme profond au fond de la fosse d'Atlantis II (Mer Rouge). Réunion Spécialisée de la Société Géol. France, Paris (abstr.).

MARSHALL, W.L. & SLUSHER, R. (1968): Solubility to 200°C of calcium sulfate and its hydrates in sea water concentrates and temperatures – concentrations limits. *Chem. Eng. Data* **13,** 83-91.

MCCLAIN, J.S., ORCUTT, J.A. & BURNETT, M. (1985): The East Pacific Rise in cross section: A seismic model. *J. Geophys. Res.* **90,** 8627-8639.

MICHARD, G., ALBARÈDE, A., MICHARD, A., MINSTER, J.F., CHARLOU, J.L. & TAN, N. (1984): Chemistry of solutions from the 13°N East Pacific Rise hydrothermal site. *Earth Planet. Sci. Lett.* **67**, 297-307.

OUDIN, E. (1983): Minéralogie de gisements et indices liés à des zones d'accrétion océaniques actuelles (ride Est-Pacifique et Mer Rouge) et fossiles (Chypre). *Chronique Rech. Minière* **470**, 43-55.

_____ (1987): Trace elements and precious metal concentrations in East Pacific Rise, Cyprus and Red Sea submarine sulfide deposits. *In* Marine Minerals (P.G. Teleki *et al.*, eds.), 349-362. Reidel Publ. Co., Dordrecht, Holland.

_____, THISSE, Y. & RAMBOZ, C. (1984): Fluid inclusion and mineralogical evidence for high-temperature saline hydrothermal circulation in the Red Sea metalliferous sediments: preliminary results. *Mar. Mining* **5**, 3-31.

PARISOD, C.J. & PLATTNER, E. (1981): Vapor–liquid equilibria of the NaCl–H_2O system in the temperature range 300–440°C. *J. Chem. Eng. Data* **26**, 16-20.

PAUTOT, G. (1983): Les fosses de la Mer Rouge: approche géomorphologique d'un stade initial d'ouverture océanique réalisée à l'aide du seabeam. *Oceanol. Acta* **6**, 235-244.

PÉCHER, A. & BOULLIER, A.M. (1984): Evolution à pression et température élevées d'inclusions fluides dans un quartz synthétique. *Bull. Minéral.* **107**, 139-153.

PITZER, K.S. & PABALAN, R.T. (1986): Thermodynamics of NaCl in steam. *Geochim. Cosmochim. Acta* **50**, 1445-1454.

_____, PEIPER, J.C. & BUSEY, R.H. (1984): Thermodynamic properties of aqueous sodium chloride solutions. *J. Phys. Chem. Ref. Data* **13**, 1-102.

POTTER, R.W., II, BABCOCK, R.S. & BROWN, D.L. (1977): A new method for determining the solubility of salts in aqueous solutions at elevated temperatures. *J. Res. U.S. Geol. Survey* **5**, 389-395.

_____, CLYNNE, M.A. & BROWN, D.L. (1978): Freezing point depression of aqueous sodium chloride solutions. *Econ. Geol.* **73**, 284-285.

POTTORF, R.J. (1980): *Hydrothermal Sediments of the Red Sea, Atlantis II Deep – A Model for Massive Sulfide Type Ore Deposits.* Ph.D. thesis, The Pennsylvania State Univ., University Park, Pennsylvania.

_____ & BARNES, H.L. (1983): Mineralogy, geochemistry and ore genesis of hydrothermal sediments from the Atlantis II Deep, Red Sea. *Econ. Geol. Monogr.* **5**, 198-223.

POTY, B., LEROY, J. & JACHIMOWICZ, L. (1976): Un nouvel appareil pour la mesure des températures sous le microscope: l'installation de microthermométrie Chaix-Meca. *Bull. Soc. franç. Minéral. Crist.* **99**, 182-186.

RAMBOZ, C. (1983): Application of V–X projections to the quantitative interpretation of heterogeneous trapping from fluid inclusion study. *Terra Cognita* **3**, 164.

_____ & DANIS, M. (1987): The temperature of the inflowing brine at the bottom of Atlantis II Deep, Red Sea. *Terra Cognita* **7**, 187.

_____, PICHAVANT, M. & WEISBROD, A. (1982): Fluid immiscibility in natural processes: use and misuse of fluid inclusion data. Part II: interpretation of fluid inclusion data in terms of immiscibility. *Chem. Geol.* **37**, 29-48.

RIDGE, J.D. (1973): Volcanic exhalations and ore deposition in the vicinity of the sea floor. *Mineral. Deposita* **8**, 332-348.

ROEDDER, E. (1972): Barite fluid inclusion geothermometry, Cartersville Mining District, Northwest Georgia. *Econ. Geol.* **67**, 821-822.

_____ (1976): Fluid inclusion evidence on the genesis of ores in sedimentary and volcanic rocks. *In* Ore in Sediments, Sedimentary and Volcanic Rocks (K.H. Wolf, ed.), **2**, 67-110. Elsevier Publ. Co.

_____ (1981): Origin of fluid inclusions and changes that occur after trapping. *In* Short Course In Fluid Inclusions: Applications to Petrology (L.S. Hollister & M.L. Crawford, eds.). *Mineral. Assoc. Can. Short Course Notes* **6**, 101-137.

ROSS, D.A. (1972): Red Sea hot brine area: revisited. *Science* **175**, 1455-1457.

_____, WHITMARSH, R.B., ALI, S.A., BOUDREAUX, J.E., COLEMAN, R., FLEISHER, R.L., GIRDLER, R., MANHEIM, F., MATTER, A., NIGRINI, C., STOFFERS, P. & SUPKO, P.R. (1973): Red Sea drillings. *Science* **179**, 377-380.

SCHOELL, M. & HARTMANN, M. (1973): Detailed temperature structure of the hot brines in the Atlantis II Deep area (Red Sea). *Mar. Geol.* **14**, 1-14.

_____ &_____ (1978): Changing hydrothermal activity in the Atlantis II Deep geothermal system. *Nature* **274**, 784-785.

SEYFRIED, W.E., JR. & JANECKY, D.R. (1985): Heavy metal and sulfur transport during subcritical and supercritical hydrothermal alteration of basalt: Influence of fluid pressure and basalt composition and crystallinity. *Geochim. Cosmochim. Acta* **49**, 2545-2561.

_____, BERNDT, M.E. & JANECKY, D.R. (1986): Chlo-

ride depletions and enrichments in seafloor hydrothermal fluids: Constraints from experimental basalt alteration studies. *Geochim. Cosmochim. Acta* **50,** 469-475.

SHANKS, W.C., III (1983): Economic and exploration significance of Red Sea metalliferous brine deposits. *In* Cameron Volume on Unconventional Mineral Deposits (W.C. Shanks, ed.). *Amer. Inst. Mining Eng. Monogr.,* 157-171.

_____ & BISCHOFF, J.L. (1977): Ore transport and deposition in the Red Sea geothermal system: a geochemical model. *Geochim. Cosmochim. Acta* **43,** 1507-1519.

SOBOLEV, V.S. & KOSTYUK, V.P., eds. (1975): Melt inclusions, their types, and thermometric methods of investigations. *In* Magmatic Crystallization Based on a Study of Melt Inclusions. Novosibirsk, Nauka Press (In Russian), translated in *Fluid Inclusion Research, Proc. of COFFI* **9,** 182-218.

SPOONER, E.T.C. (1980): Cu–pyrite mineralization and sea water convection in oceanic crust. The ophiolitic ore deposits of Cyprus. *Geol. Assoc. Can. Spec. Pap.* **20,** 685-704.

SVAL'NOV, N., STRIZHOV, V.P., BOGDANOV, Y.A. & ISAYEVA, A.B. (1984): Hydrothermal barite crust on basalts in Atlantis II Deep (Red Sea). *Oceanology* **24,** 716-720.

THISSE, Y. (1982): *Sédiments Métallifères de la Fosse d'Atlantis II (Mer Rouge). Contribution à l'Étude de Leur Contexte Morpho-Structural et de Leurs Caratéristiques Minéralogiques et Géochimiques.* Ph.D. thesis, Université Orléans et B.R.G.M., Orléans, France.

THOMPSON, J.B., JR. (1972): Oxides and sulfides in regional metamorphism of pelitic schists. *24th Int. Geol. Congress, Section* **10,** 27-35.

TURNER, J.S. (1969): A physical interpretation of the observations of hot brine layers in the Red Sea. *In* Hot Brines and Recent Heavy Metal Deposits in the Red Sea (E.T. Degens & D.A. Ross, eds.). Springer-Verlag, Berlin, 164-173.

URUSOVA, M. (1974): Phase equilibria in the sodium hydroxide – water and sodium chloride – water systems at 350–550°C. *Russian J. Inorg. Chem.* **19,** 450-454.

VANKO, D.A. (1984): Chlorine-rich amphiboles and chlorine-rich fluid inclusions in quartz: Evidence for high salinity oceanic hydrothermal systems. *Geol. Soc. Amer. Program Abstr.* **16,** 682.

VOORHIS, A.D. & DORSON, D.L. (1975): Thermal convection in the Atlantis II hot brine pool. *Deep-Sea Research* **22,** 167-175.

VON DAMM, K.L., EDMOND, J.M., MEASURES, C.I., GRANT, B.C., TRULL, T., WALDEN, B. & WEISS, R. (1985): Chemistry of submarine hydrothermal solutions at 21°N, East Pacific Rise. *Geochim. Cosmochim. Acta* **49,** 2197-2221.

WEISBROD, A. (1984): Utilisation des inclusions fluides en geothermobarométrie. *En* Thermométrie et Barométrie Géologiques (M. Lagache, ed.). *Bull. Soc. franç. Minéral. Crist.* **2,** 1016-1027.

WEISS, H. M., NÖLLTNER, T. & STOFFERS, P. (1980): Occurrence of ilvaite in metalliferous brine muds from the Red Sea. *Neues Jahrb. Mineral. Abh.* **139,** 239-253.

WILKINS, R.W.T. & SVERJENSKY, D.A. (1977): The role of fluid inclusions in the exsolution of clinopyroxene in bustamite from Broken Hill, New South Wales, Australia. *Amer. Mineral.* **62,** 465-474.

WHITE, D.E. (1968): Hydrology, activity, and heat flow of the Steamboat Springs thermal system, Washoe County, Nevada. *U.S. Geol. Surv. Prof. Pap.* **458-C.**

YAJIMA, J. & TOURAY, J.C. (1967): Observation sur la sursaturation des liquides inclus dans les cristaux de fluorite. *C.R. Acad. Sci., Paris* **264,** 1129-1132.

ZHANG, Y.G. & FRANTZ, J.D. (1987): Determination of the homogenization temperatures and densities of supercritical fluids in the sytem NaCl-KCl-H_2O using synthetic fluid inclusions. *Chem. Geol.* **64,** 335-350.

ZIERENBERG, R.A. & SHANKS, W.C., III (1983): Mineralogy and geochemistry of epigenetic features in metalliferous sediments, Atlantis II Deep, Red Sea. *Econ. Geol.* **78,** 57-72.

_____ & _____ (1986): Isotopic constraints on the origin of the Atlantis II, Suakin and Valdivia brines, Red Sea. *Geochim. Cosmochim. Acta* **50,** 2205-2214.

Received January 29, 1988; revised manuscript accepted June 9, 1988.

APPENDIX

Significance of fluid-inclusion data in anhydrite

Anhydrite, like all soft, cleaved minerals, is susceptible to stretching (Larson *et al.* 1973). Fluid inclusions in anhydite often yield high and scattered T_h. Similar distributions in barite have been attributed to non-systematic behavior of the inclusions during heating runs (Roedder 1972). Numerous problems were encountered in the study of fluid inclusions in

Red Sea anhydrite. Many inclusions burst prior to homogenizing. Inclusions that changed shape by precipitating anhydrite on heating were observed once. Nevertheless, we believe that stretching problems have been minimized in this study; 80% of the phase changes were measured twice. About 5% of the microthermometric measurements were also repeated after the samples had been stored for one year at room temperature. As reproducible measurements were obtained, the crystals therefore had remained unchanged even though anhydrite in contact with the ≈ 6 molal NaCl solution from the inclusions is unstable and should transform to gypsum at room temperature (Marshall & Slusher 1968). Figure 12 shows that inclusions in anhydrite, whatever their size, have high, scattered T_h values. This implies that stretching alone cannot account for all the high T_h values because, with stretching, the largest inclusions should exhibit the highest T_h values (Bodnar & Bethke 1984).

Re-equilibration of the Red Sea anhydrite can also complicate the interpretation of the microthermometric data. Brine venting has been active from the Holocene to the present in the SW Basin of the Deep. Anhydrite crystals in sediments from that part of the basin may therefore have been repeatedly reheated, even if the crystals are very young (*e.g.*, Cole 1983). Both the tubular inclusions with round ends in the anhydrite cores, and the more isometric type-*S* inclusions with sharp angles near the crystal margins, are sensitive to re-equilibration (Pécher & Bouiller 1984, Gratier & Jenatton 1984, Doukhan & Trépied 1985). Type-*L* and *V* inclusions often root on solid microinclusions; such associations may act as defects in the lattice, along which re-equilibration processes are initiated (Wilkins & Sverjensky 1977). Nevertheless, the shape of the inclusions in the Red Sea anhydrite indicates that the crystals have not been re-equilibrated at the temperature of the surrounding sediments. Besides, the anhydrite has trapped boiling fluids, *i.e.*, fluids coexisting on the liquid–vapor curve. The trapping pressure indicated by fluid inclusions is consistent with the depth of the crystals beneath sea level.